NATIONAL ADVISORY COMMITTEE FOR AERONAUTICS

TECHNICAL NOTE 4325

A MACH 4 ROCKET-POWERED SUPERSONIC TUNNEL USING AMMONIA-OXYGEN AS WORKING FLUID

By Robert W. Graham, Eleanor Costilow Guentert, and Vearl N. Huff

Lewis Flight Propulsion Laboratory
Cleveland, Ohio

Washington
September 1958

NATIONAL ADVISORY COMMITTEE FOR AERONAUTICS

TECHNICAL NOTE 4325

A MACH 4 ROCKET-POWERED SUPERSONIC TUNNEL USING AMMONIA-OXYGEN AS WORKING FLUID

By Robert W. Graham, Eleanor Costilow Guentert, and Vearl N. Huff

SUMMARY

A rocket-powered supersonic tunnel has been constructed to simulate the high heating rates encountered in hypersonic flow. A gas temperature of 4500° R at Mach 4 has been produced in the 15-inch test section of the tunnel. The calibration pressure data indicate reproducibility of test conditions in this facility.

Physical, transport, and one-dimensional aerodynamic data for combustion products of ammonia and oxygen are included.

INTRODUCTION

The increasing demands for flight at hypersonic speeds has introduced an acute problem which is frequently referred to as "aerodynamic heating" or the "thermal barrier." The excessive temperature generated by the frictional action of air at hypersonic speeds produces deleterious effects upon materials and structures. The heat-transfer mechanism at these elevated temperatures differs from that normally encountered in fluid flow in that dissociated gases may recombine at the surface and liberate considerable amounts of heat. Several papers (refs. 1 to 3), have discussed the heat-transfer problem with dissociation in the boundary layer.

New types of research facilities and techniques are required for experimental studies of heat transfer at hypersonic speed. An apparatus to meet this need is a high temperature - high Mach number tunnel in which the exhaust gases from a chemical rocket are the working fluid. This type of tunnel, which utilizes the combustion products of ammonia and oxygen, has been constructed at the NACA Lewis laboratory. A description and evaluation of a cylindrical 15-inch rocket tunnel as a suitable facility for obtaining heat-transfer data in a hot gas stream are presented herein.

DESCRIPTION OF TUNNEL

The principal components of the rocket tunnel are: (1) the rocket which is the source of high temperature gas, (2) the divergent section where the gas expands to a high velocity, and (3) the constant-diameter straight sections, which serve as the test section. A sketch of the entire rocket tunnel is shown in figure 1. The tunnel assembly was free to move in the axial direction.

The tunnel uses the exhaust of an ammonia-oxygen rocket motor as a source of working gas. This particular propellant combination was selected because the combustion products were nontoxic, noncorrosive, and can comprise an oxidizing atmosphere.

The exhaust products from the combustion of oxygen and ammonia are tabulated in detail in reference 4. Some typical values for the exhaust species at a chamber pressure of 600 pounds per square inch absolute are listed in the following table. All of these data were computed assuming equilibrium composition. The data at 3 pounds per square inch absolute are typical of the composition in the tunnel test section.

Composition	Static pressures, $\frac{lb}{sq\ in.}$ abs	Temperature, °K	Mole fraction							
			H_2	H_2O	N_2	OH	O_2	NO	H	O
Stoichiometric	600	2980	0.0481	0.6389	0.2367	0.0567	0.0078	0.00513	0.0051	0.0014
	300	2768	.0364	.6672	.2404	.0423	.00624	.0035	.0031	.0008
	3	1425	.00016	.7497	.2500	.00013	.00004	0	0	0
20 Percent excess oxygen	600	2914	0.0148	0.6218	0.2199	0.0779	0.0491	0.0114	0.0023	0.0029
	300	2689	.0087	.6442	.2233	.0593	.0529	.0087	.0011	.0017
	3	1308	0	.6975	.2325	.0003	.0696	.0001	0	0

Property data for the combustion products are contained in an appendix.

The divergent portion of the rocket nozzle is extended to expand the flow to a Mach number of approximately 4.0 at the test section. A total temperature of approximately 4500° R was obtained at the tunnel test section. At this temperature there is a small amount of dissociation in the boundary layer.

A rocket tunnel poses unique problems, some of which are: (1) selection of a propellant combination that contains a minimal amount of

toxic, corrosive, and carbonaceous products, (2) accurate determination of the thermodynamic properties of the products of combustion, (3) development of a special rocket-starting technique because the tunnel addition to the rocket nozzle eliminates any igniting systems that initiate at the original rocket exit, (4) development of special temperature and pressure instrumentation for the high temperature - high Mach number tunnel operating conditions, and (5) adequate cooling for the tunnel with sufficient tunnel access ports and visual and instrumentation holes.

The maximum diameter of the tunnel was selected to conform to a near-maximum expansion that could take place with atmospheric back pressure at the tunnel exit. It was presumed that recovery to atmospheric pressure would take place across a normal shock at the tunnel exit. Subsequent data have indicated the presence of this normal shock at the tunnel exit. The area ratio for the tunnel is 33.2.

Rocket

The rocket motor is a 5000-pound-thrust, ammonia-oxygen rocket with a throat diameter of 2.65 inches and a chamber pressure of 600 pounds per square inch absolute. Ignition is accomplished with a propane torch at the injector end of the combustion chamber. The torch tube was introduced through the injector face or through the walls of the combustion chamber near the injector face. The latter arrangement was the most satisfactory.

Two types of injectors were utilized in the rocket. The first was an injector in which the nozzles sprayed fuel in a like-on-like pattern and sprayed the oxidizer in a showerhead pattern. This particular injector was known to be less efficient than other types but was considered less likely to cause burnout problems. The second injector was built with like-on-like nozzles for both the fuel and oxidizer. This design raised the combustion temperature approximately 300° F above that of the first injector.

Divergent Section

The divergent nozzle was water cooled. Double-wall construction was necessary to provide a cooling jacket around the nozzle wall. The inner surface of the wall was contoured to a prescribed aerodynamic shape. The coolant-side or outer surface of the wall was also machined to keep the wall thickness constant for cooling purposes.

The area ratio A/A_t as a function of axial distance along the divergent section is shown in figure 2. (All symbols are defined in appendix A.) The contour was designed by using a one-dimensional flow

theory. Application of the method of characteristics to this design problem would be complicated by the thermochemical state of the high energy gases. The pressure exponent of the gases is not the ratio of specific heats when the gas is in an elevated energy state, but is a function of the partial derivative of the molecular weight with respect to the pressure.

The profile-contour of the divergent section made it difficult to fabricate a water jacket out of sheet metal. A water jacket was fabricated from laminations of polyester resin and glass fiber cloth. The jacket was shaped by coating the outside surface of the machined shell with a constant thickness of wax. Then alternating layers of cloth and resin were wrapped around the wax until the laminated sheath was about 0.090 inch thick. The wax was baked out leaving a constant thickness of water passage between the divergent-section shell and the plastic jacket.

To be conservative on coolant requirements, the divergent section was designed to withstand heat flux densities as great as the rocket nozzle. The heat flux density was estimated to be 2.0 Btu per second per square inch at the small diameter end of the divergent section. A design wall temperature of 900° F was selected for the inner surface. The wall was cooled with a water jacket in which the water passages were helical paths formed by winding copper tubes around the inner wall of the section. The copper tubes did not carry any coolant; rather the outside surface of the tubes acted as walls for guiding the coolant in a spiral path. The purpose of the spiraled paths is to give the water high velocities and, thus, a higher Reynolds number for effective cooling. The same type of coolant-passage design was used in the rocket motor, in which the coolant requirements were more severe than at any other location in the tunnel.

Straight Section

In order to simplify fabrication, the straight test section was divided into two water-cooled sections, each 3 feet in length. Each section was fabricated from pieces of Inconel rolled plate that were welded together to form a cylinder. The inner and outer surfaces were machined; the inner surface to a 64 microinch finish. As is shown in figure 1, window ports were installed in the upstream section and 12 static taps were located at equal axial spacings over the straight part of the tunnel.

RESULTS AND DISCUSSION

Calibration Tests

To calibrate the tunnel, a series of runs was completed in which the total- and static-pressure profiles of the tunnel were determined. A description of the pressure instrumentation appears in appendix B. The total-pressure rake used is shown in figure 3. To evaluate the resistance of the conical tips of models introduced in the tunnel, uncooled tips were placed in the tunnel during several of the calibration runs. Figure 4 illustrates what happened to a sharp Inconel cone after 10 seconds of exposure to the tunnel gases. Blunted uncooled shapes suffered little surface errosion up to about 3 seconds of exposure.

During the calibration runs, the length of run was gradually increased from 3 seconds to 13 seconds. After each incremental increase in time of run, the tunnel was carefully inspected for signs of thermal damage.

Figure 5 shows the total pressure measured at the inlet of the tunnel straight sections as a function of the radial dimension of the tunnel. These data were obtained with the total-pressure rake described in appendix B and are behind a normal shock (produced by the rake). The data indicate a reversed total-pressure gradient in the tunnel. Possible reasons for this reversed gradient will be pointed out in subsequent discussion.

Figure 6 presents the static-pressure profile along the axial dimension of the tunnel. These data were obtained during the early runs of the tunnel. Fair reproducibility of the static pressures was obtained at each axial station for this series of runs. Subsequent runs have produced differently shaped pressure profiles. These differences have been attributed to:

(1) Performance differences in the rocket combustion caused by replacement injectors and combustion chambers,

(2) Appreciable wavy-wall effects on the gas flow as the result of cumulative effects of thermal stresses on the tunnel walls and the expansion nozzle (measurements of the surfaces indicated buckles as deep as 0.030 in. in the nozzle after 60 runs), and

(3) Lips or steps in the joints of the three matching pieces constituting the tunnel. Thermal effects caused the circular cross-section of the tunnel pieces to distort into an elliptical shape, thus producing steps where the pieces were joined.

The rocket performance data indicate that the combustion temperature is approximately 4500° R. The total temperature measured at the inlet of the rocket tunnel test section with a pneumatic probe (ref. 5) also indicates a total temperature of 4500° R.

As a part of the tunnel calibration, schlieren photographs of the shock waves from a double-angle wedge were made to determine the Mach number of the tunnel. A reproduction of a frame from the schlieren motion pictures is shown in figure 7. The wedge used in these tests was constructed with a slightly blunted edge because the theoretically desirable sharp edge could not be cooled. Blunting undoubtedly affects the accuracy of this technique. By virtue of the two different angles on the wedge, an approximate estimation of the variation of shock angle with wedge angle can be determined and the Mach number computed. The Mach number obtained in this manner varied from 3.5 to 4.0. The variation in the data was attributed to optical difficulties with the schlieren system and to changes in the wedge geometry caused by severe heating. The schlieren tests, which were deemed to be the most reliable of the group, produced Mach number data within the range of 3.6 to 3.8.

Determination of the Mach number from experimental data necessitated use of one-dimensional gas flow information, normal shock data, and thermodynamic properties of the products of combustion of ammonia and oxygen. These data appear in figures 8 and 9 and additional useful ammonia-oxygen data appear in appendix C. The normal shock and gas dynamics data were computed for three mixture ratios; stoichiometric, 10-percent excess oxygen, and 20-percent excess oxygen. The transport data were computed for stoichiometric and 20-percent excess oxygen mixtures. The thermodynamic data were computed for a wide range of mixture ratios. However, during most of the calibration runs, the tunnel was operated with 20-percent excess oxygen.

The Mach number for isentropic expansion in the tunnel was 4.2 using the area ratio of 33.2 (fig. 8(a), area ratio as a function of Mach number for 20-percent excess oxygen) at the end of the divergent section.

If the curve of static pressure plotted against Mach number for a chamber pressure of 40 atmospheres was employed (fig. 9(a)), a Mach number of 3.6 was obtained at the entrance to the constant-diameter test section of the tunnel. Employing the normal shock data of figure 10 for 20-percent excess oxygen, the Mach number was 4.25. The Mach numbers obtained from the one-dimensional flow computations are summarized in the following table:

Method		Mach number
Schlieren - double angle wedge		3.6 to 3.8
Area ratio, A_t/A_e	100% Combustion efficiency	4.2
Static pressure		3.6
Normal shock		4.25

The gas dynamics and normal shock data in appendix C were developed assuming ideal combustion conditions. Inasmuch as the observed combustion efficiency of the rocket combustor was approximately 90 percent, a thermodynamic system was devised incorporating the effects of incomplete combustion.

The incomplete combustion constituents were simulated by inert nitrogen species. The thermodynamic system consisted of ammonia, oxygen, and nitrogen with a calculated amount of the inert nitrogen present to produce a combustion efficiency corresponding to the measured value of 90 percent.

Assuming a total pressure of 600 pounds per square inch absolute, the relation of Mach number to static pressure for incomplete combustion is shown in figure 11. The wall static-pressure data at the inlet of the straight test section showed a static pressure of approximately 3.5 pounds per square inch absolute, thus the Mach number of the tunnel gases was 3.85.

The pressure sensed by the total pressure rake is the total pressure behind a normal shock. To compute the conditions behind a normal shock from conditions upstream of the shock, simultaneous solution of the momentum and continuity equations is required. Neglecting any losses, the total momentum (pressure and velocity forces) upstream of the shock equals the vacuum specific impulse of the rocket. Employing the thermodynamic data of the ammonia-oxygen-nitrogen model of the real combustion gases, the computed vacuum specific impulse agrees with the experimental value, as shown in figure 12. The experimental vacuum specific impulse was computed by adding the pressure force to the measured thrust. A simultaneous solution of the continuity and impulse equation revealed that the total pressure behind the shock was 30 pounds per square inch absolute. This value agreed with the average experimental value. The incomplete combustion phenomena probably explains the reversed radial gradient of total pressure; that is, higher total pressures existed at the wall than in the center of the tunnel. However, another possible explanation of the reversed radial gradient is the stratification of the unburned gases. One gas sampling experiment indicated considerable stratification in the flow near the wall.

The radial gradients of total pressure may also be caused by shock waves originating in the nozzle and intersecting the face of the pressure rake. Judging from the static-pressure distribution in the tunnel (fig. 6) there are appreciable pressure losses in the tunnel. Shocks appear at axial stations 34 and 58 inches from the inlet of the constant diameter section, as indicated by the static-pressure rise at these stations.

The existence of these shock waves in the tunnel in part may be attributed to the fact that the tunnel expansion section does not have the correct aerodynamic shape. As mentioned in the description of the tunnel, no rigorous aerodynamic design technique was applied in prescribing the contour of the expansion nozzle. For a shock-free flow field, it would be necessary to apply complicated gas dynamics equations to the design of the nozzle. The analytical technique would have to comprehend the reaction rates of the high temperature gases as well as the equations of motion and energy for supersonic flow. The absolute success of such a design procedure is contingent upon an accurate model of the reactions of the gaseous species.

Heat-Transfer Data

An important phase in the evaluation of the tunnel is the fundamental heat-transfer data obtained from a body of revolution suspended in the tunnel.

The model used for the heat-transfer measurements is shown in figure 13. It was 4 feet long, 5 inches in diameter, and contained 12 thermocouples and pressure taps. The tunnel runs with this uncooled model were necessarily short to prevent thermal damage. The temperature-time records were extrapolated to steady-state conditions. The computed heat-transfer coefficients for the gas film are shown in figure 14. The curves represent the predicted heat-transfer coefficients for the laminar and turbulent boundary layers according to the theories of Chapman, Rubesin, and Van Driest.

The data indicate that laminar flow was present at the nose of the model and transition occurred 8 to 10 inches downstream from the tip. The scatter in the turbulent data is attributed to shock patterns impinging on the model.

Evaluation of the Rocket Tunnel

The pressure data indicate that the tunnel is not perfect aerodynamically. The incorrect nozzle shape caused the shock losses observed in the early experimental runs. Repeated use of the tunnel produced thermal distortions of the components, which further aggravated the shock

losses. It is apparent in operating hot gas tunnels that thermal distortions will affect the aerodynamic performance of the tunnel. Another general observation concerning hot gas tunnels derived from experience with the rocket tunnel concerns the measurement of the thermodynamic state of the gases. During the expansion process, the composition of the gases varies appreciably, thus it is difficult to relate such variables as total pressure and static pressure by means of one-dimensional gas relations. All of these relations involve the isentropic exponent γ, which varies with gas composition and temperature.

The static- and total-pressure data indicate reproducibility of test conditions within the tunnel.

CONCLUDING REMARKS

The cylindrical 15-inch rocket tunnel was designed for heat-transfer measurements. The heat-transfer data presented in figure 14 indicate fair correlation with the theoretical information. Judging from these data and despite an imperfect flow field, it is concluded that the tunnel is a useful apparatus for heat-transfer studies. Redesign of the expansion nozzle will reduce the undesirable shock losses in the tunnel. However, the appreciable differences in physical and transport properties between the rocket exhaust gases and air make correlation of aerodynamic heating data difficult.

The tunnel has been useful in examining the thermal-resistance qualities of materials and coatings on surfaces, which must withstand severe aerodynamic heating.

An excess of oxygen in the combustion products of the rocket can be used to support combustion in a burner model located in the test section. Consequently, the tunnel can be used to investigate the problems of combustion in high Mach number ramjet burners.

Lewis Flight Propulsion Laboratory
National Advisory Committee for Aeronautics
Cleveland, Ohio, June 20, 1958

APPENDIX A

SYMBOLS

A	area
a	speed of sound
C_p	specific heat at constant pressure
c*	characteristic velocity, ft/sec
h	heat-transfer coefficient, Btu/(sec)(sq ft)($^\circ$R)
I	impulse, $\frac{\text{lb-sec}}{\text{lb}}$
O/F	oxygen to fuel ratio, by weight
P	total pressure
p	static pressure
Pr	Prandtl number
t	static temperature
x	axial distance along tunnel
γ	isentropic exponent
μ	dynamic viscosity
ρ	density

Subscripts:

c	chamber
e	exit
t	throat

w wall

∞ free stream

APPENDIX B

PRESSURE INSTRUMENTATION

Total-Pressure Rake

The total-pressure profile across the tunnel was measured with a water-cooled total-pressure rake shown in figure 3. The rake, fabricated from welded 1/8-inch Inconel plate, was long enough to survey one-half the tunnel diameter when mounted in an instrument port. The leading edge was contoured with a 3/8-inch radius. The five tips housing the total-pressure taps were fabricated from copper to enhance conduction cooling effects. Initially, conduction was the only means for cooling the tips. This proved to be an inadequate means of cooling, so water was circulated through the tip and expelled through an annular orifice near the inlet of the pressure tap. The addition of the water coolant effectively prevented burning of the pressure taps and permitted repetitive runs with no appreciable damage to the probe. In order to cool the body and the pressure-sensing tips of the probe, 4 pounds of water per second were required. The total pressures were sensed by Statham transducers and were recorded simultaneously on a multichannel oscillograph.

Experience with Materials for Total-Pressure Rake

Various materials were used in the fabrication of the pressure-sensing tips of the total-pressure rake. The body of the probe was cooled by high pressure water but cooling of the tips was dependent on the conduction properties of the tip material. Consequently, a highly conductive material such as copper was chosen for the tips of the first probe built. The first probe was exposed to the hot gases of the tunnel for approximately 4 seconds. The tips, which were cylindrical and extended 3/4 inch beyond the front face of the probe, were almost totally burned. The front face of the probe was irreparably damaged.

As the result of this first experience, the next probe was designed with greater coolant-flow capacity and with a greatly accelerated fluid velocity along the front face of the probe. The new copper tips were tapered so that the cross-sectional area at the base of the tips was greater than that at the ends, to compensate for the greater conduction load required of the base section in transferring the heat from the ends of the tip.

The modified total-pressure rake was exposed to the hot tunnel gases for approximately 5 seconds and seemed to hold up much better than the first design. However, the copper tips were still severely burned and the bow waves off the tips erroded the face of the probe.

In an attempt to find a material for the tips that would be better than copper, probes were fabricated in which each tip was of a different material. At least one copper tip was incorporated in each probe to allow a comparison of the various tip materials with the known performance of the copper tips.

Inconel. - Despite the poor conductivity of Inconel, trial tips of this material were tested because Inconel is a highly heat-resistant material. The Inconel tips were made of standard 1/8-inch tubing. These tips did not stand up as well as the copper tips.

Molybdenum disilicide. - Tips were made from 1/8-inch tubing of molybdenum disilicide. The lack of physical strength made this material subject to physical failure so it was entirely unacceptable without some sort of sleeve to strengthen it. Molybdenum disilicide tubing inserts were tried in graphite and copper tips, but the failure of the tubes blocked the aspirating passage of the probe. The material does exhibit considerable resistance to burning at elevated temperatures but lacks strength.

Static-Pressure Measurement

Twelve static-pressure taps were provided at 6-inch intervals along the tunnel straight sections as indicated in figure 1. The static pressure was sensed by a calibrated high-frequency response, variable-inductance pressure gage.

Appreciably long pressure lead lines to the transducers, traps to condense ammonia vapors, and a manifold pincher system caused the volume of the static-pressure system to be undesirably great resulting in an appreciable time lag of 5 seconds.

Tunnel Thermocouples

Two iron-constantan thermocouples for measuring the tunnel wall temperature were located at either end of the straight sections, as indicated in figure 1. The thermocouples were in contact with the coolant side of the tunnel wall. Tunnel wall safety limits of 400° F were set on all thermocouples, which would terminate the rocket run automatically.

APPENDIX C

ONE-DIMENSIONAL GAS FLOW, AND THERMODYNAMIC PROPERTIES FOR AMMONIA-OXYGEN SYSTEM

Data appear in this report concerning the thermodynamic and transport properties of ammonia-oxygen systems as well as rocket performance parameters. The following figures are involved:

Static pressure, density, and temperature relations for ammonia-oxygen combustion products for 20 percent, 10 percent, and stoichiometric conditions are presented in figure 15. Sonic velocity and Mach number as a function of static temperature for ammonia-oxygen combustion products for 20 percent, 10 percent, and stoichiometric conditions are presented in figure 16. Specific heat data over a range of static temperatures for ammonia-oxygen combustion products for 20 percent, 10 percent, and stoichiometric conditions are given in figure 17. In figure 18, the transport data for ammonia-oxygen at 20-percent excess oxygen and stoichiometric conditions are given. The specific impulse of ammonia-oxygen at P_c = 600 pounds per square inch absolute for frozen and equilibrium conditions is given in figure 19. The combustion temperature of ammonia-oxygen over a range of mixture ratios for frozen and equilibrium conditions is given in figure 20. In figure 21, the area ratio as a function of mixture ratio for ammonia and oxygen for frozen and equilibrium conditions is presented. The characteristic velocity as a function of mixture ratio for ammonia-oxygen for frozen and equilibrium compositions is shown in figure 22. In figure 23, the isentropic exponent as a function of mixture ratio for ammonia and oxygen for frozen and equilibrium conditions is given.

REFERENCES

1. Van Driest, E. R.: The Problem of Aerodynamic Heating. Aero. Eng. Rev., vol. 15, no. 10, Oct. 1956, pp. 26-41.

2. Bond, J. W., Jr.: Problems of Aerophysics in Hypersonic Region. Aero. Digest, vol. 72, no. 6, June 1956, pp. 21-25.

3. Altman, D., and Wise, H.: Effect of Chemical Reactions in the Boundary Layer on Convective Heat Transfer. Jet Prop., vol. 26, no. 4, Apr. 1956, pp. 256-258; 269.

4. Gordon, Sanford, and Glueck, Alan, R.: Theoretical Performance of Liquid Ammonia with Liquid Oxygen as a Rocket Propellant. NACA RM E58A21, 1958.

5. Simmons, Frederick S., and Glawe, George E.: Theory and Design of a Pneumatic Temperature Probe and Experimental Results Obtained in High Temperature Gas Stream. NACA TN 3893, 1957.

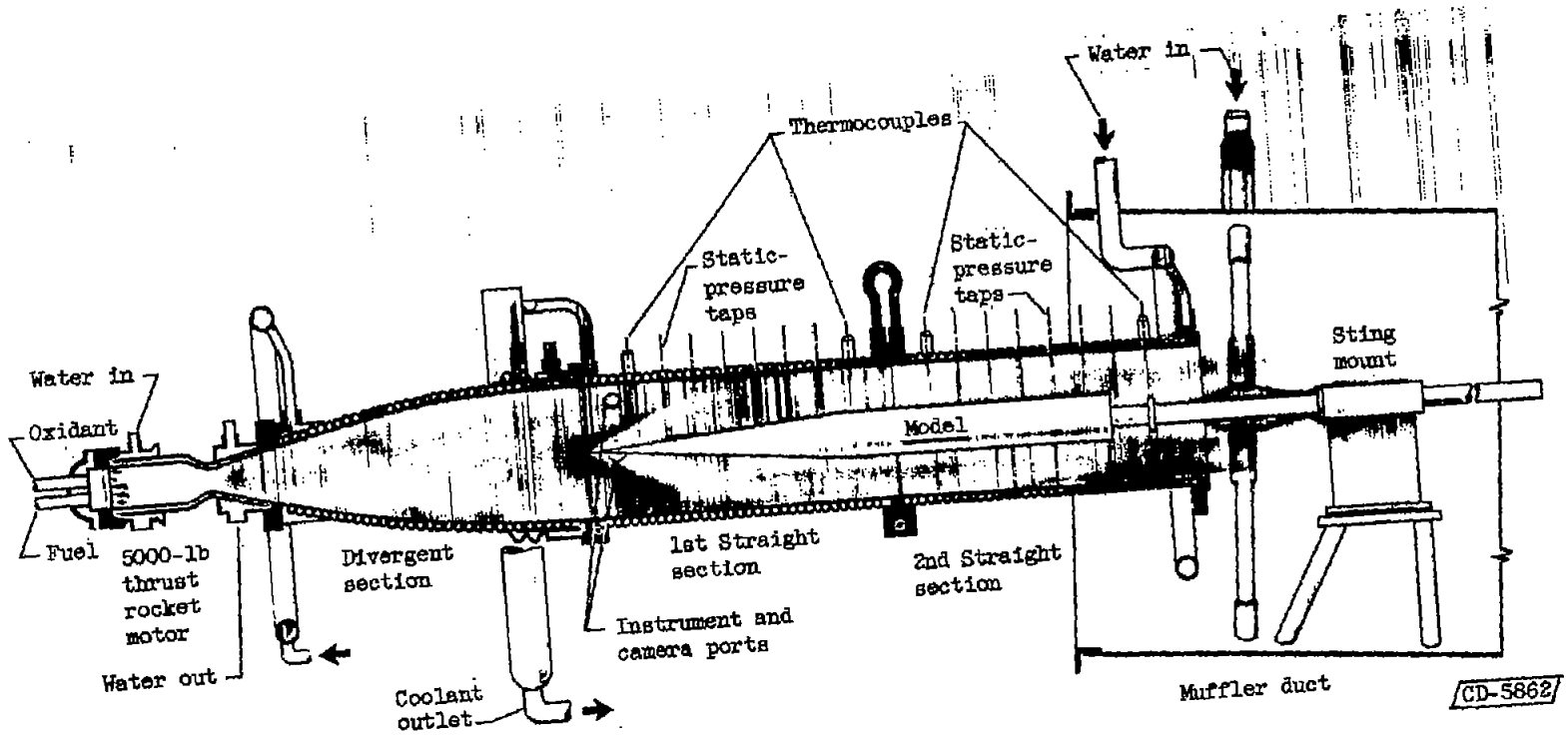

Figure 1. - Rocket tunnel.

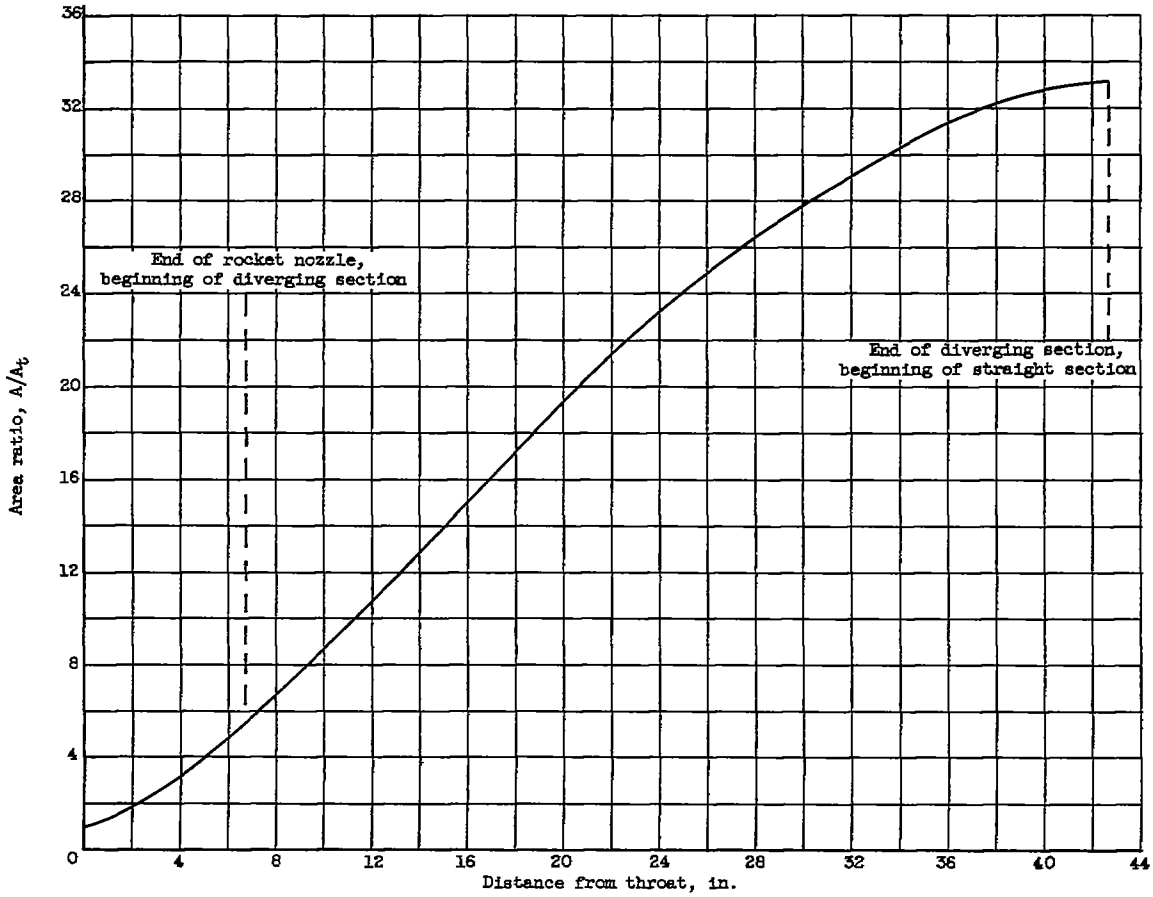

Figure 2. - Area ratio distribution as a function of nozzle length for rocket tunnel.

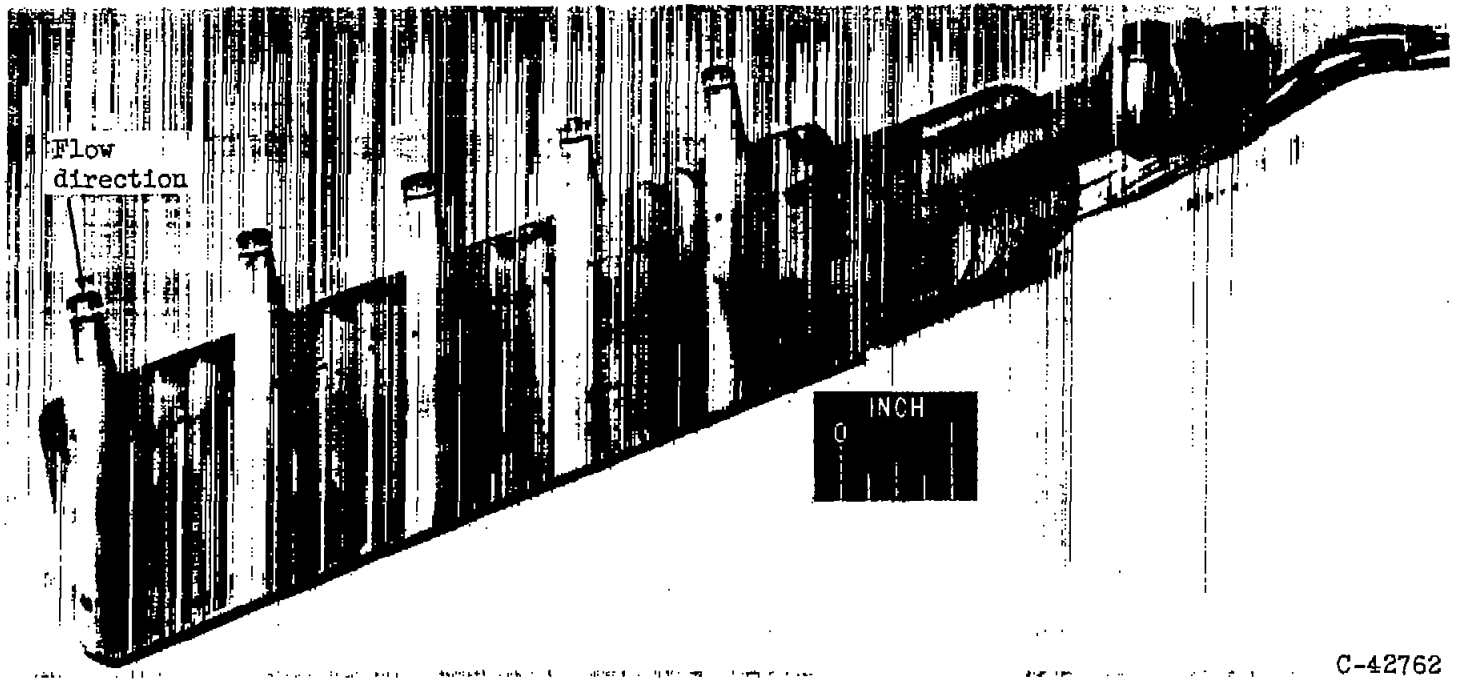

C-42762

Figure 3. - Total-pressure rake.

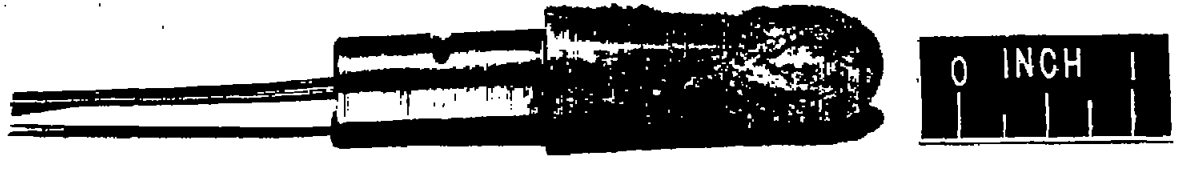

C-42704

Figure 4. - Initially sharp-tipped cone after 10-second exposure to tunnel gases.

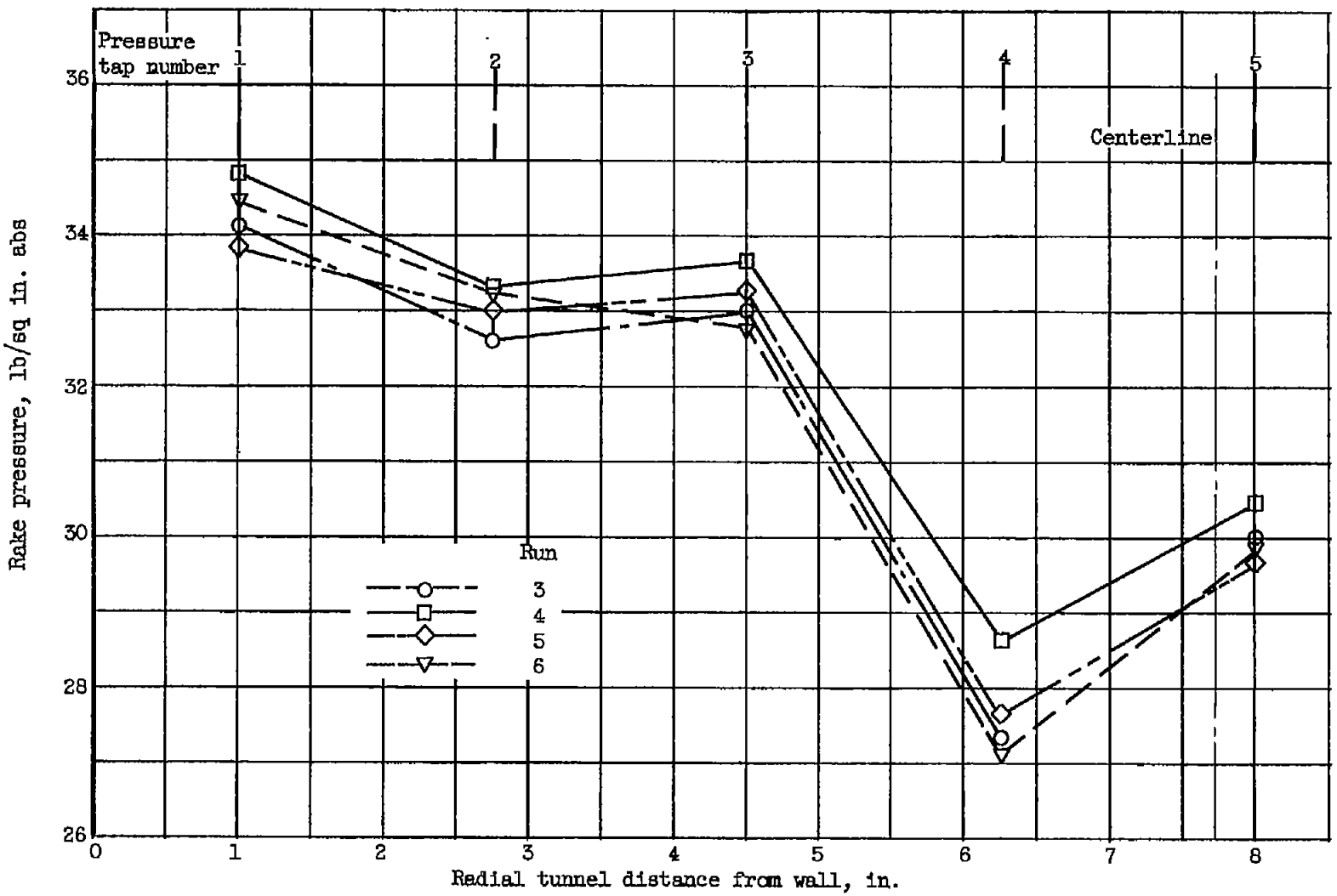

Figure 5. - Total-pressure profile at inlet of constant-diameter section.

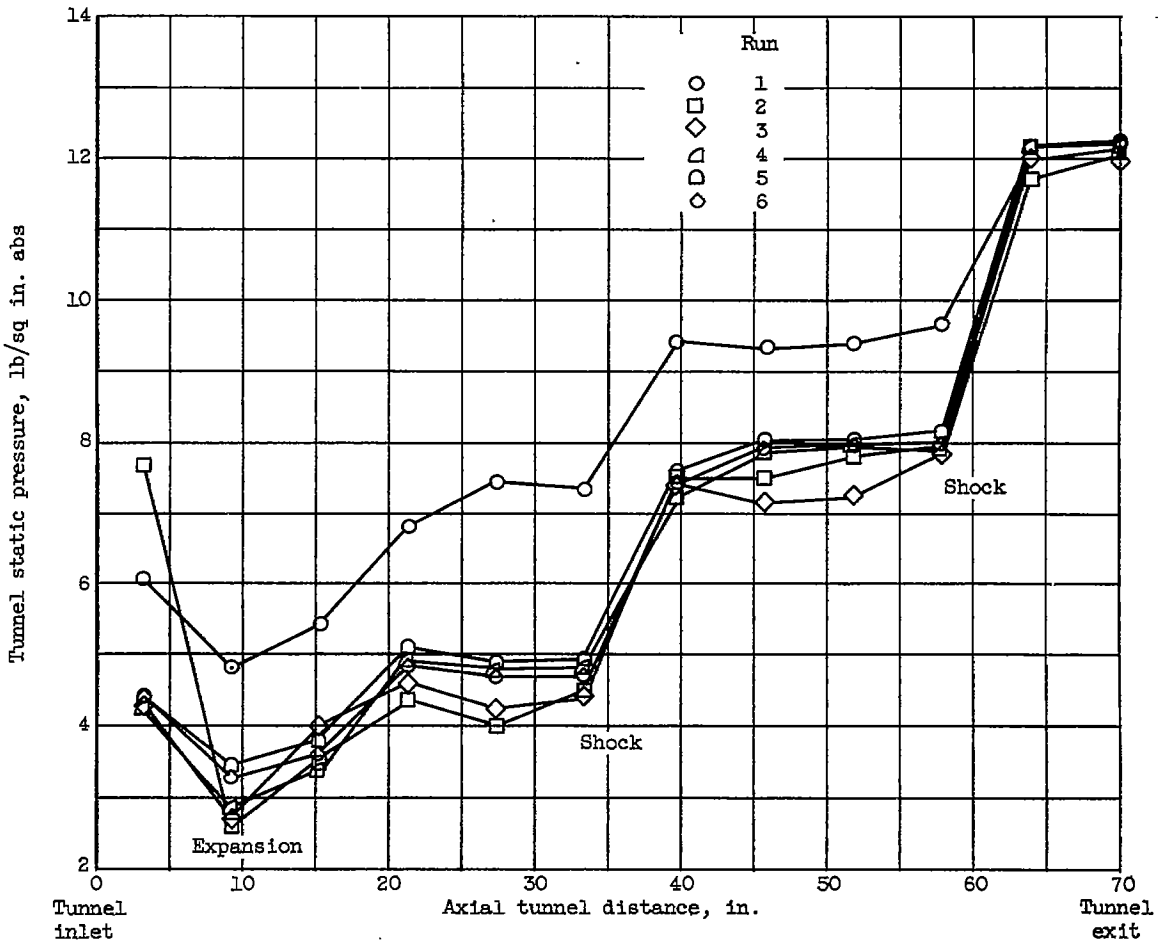

Figure 6. - Tunnel static-pressure profile.

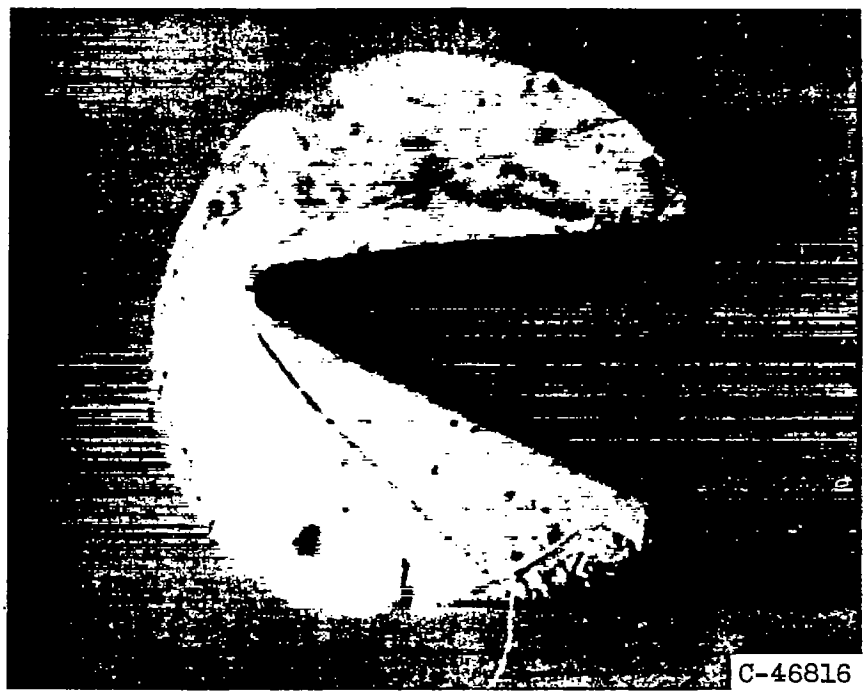

Figure 7. - Schlieren photograph of wedge in rocket tunnel.

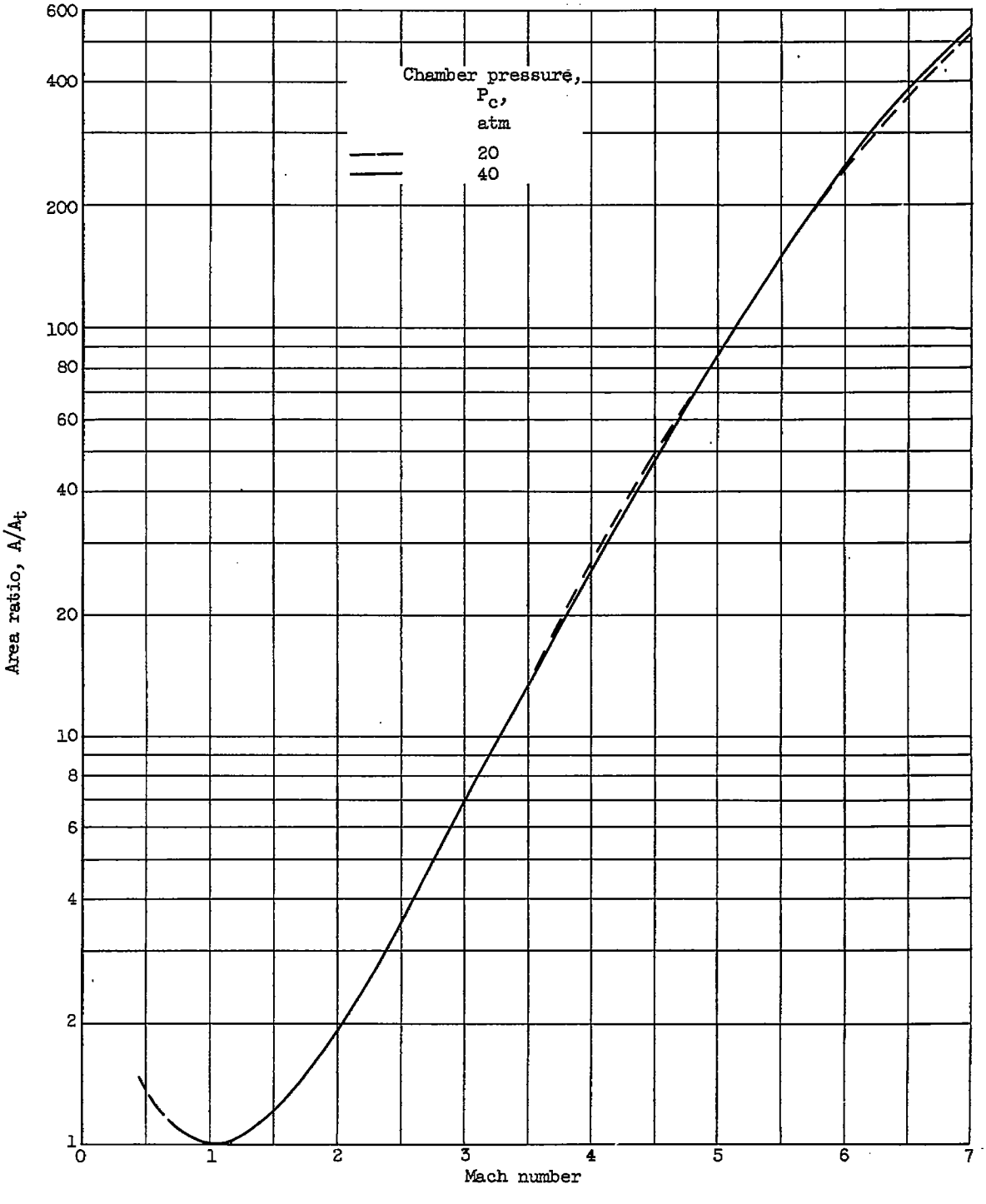

(a) Excess oxygen, 20 percent.

Figure 8. - Relation of one-dimensional area ratio and Mach number for ammonia-oxygen combustion gases.

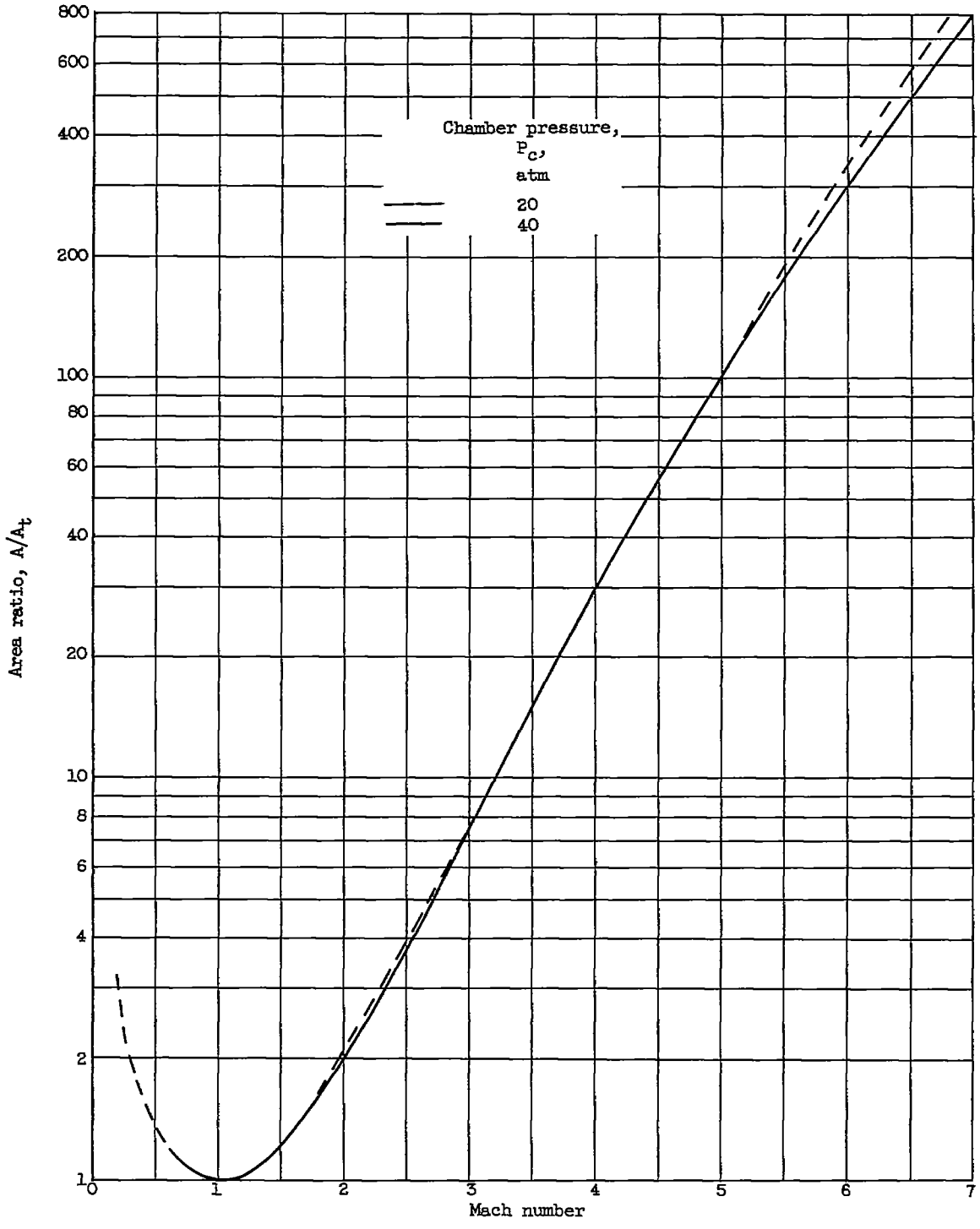

(b) Excess oxygen, 10 percent.

Figure 8. - Continued. Relation of one-dimensional area ratio and Mach number for ammonia-oxygen combustion gases.

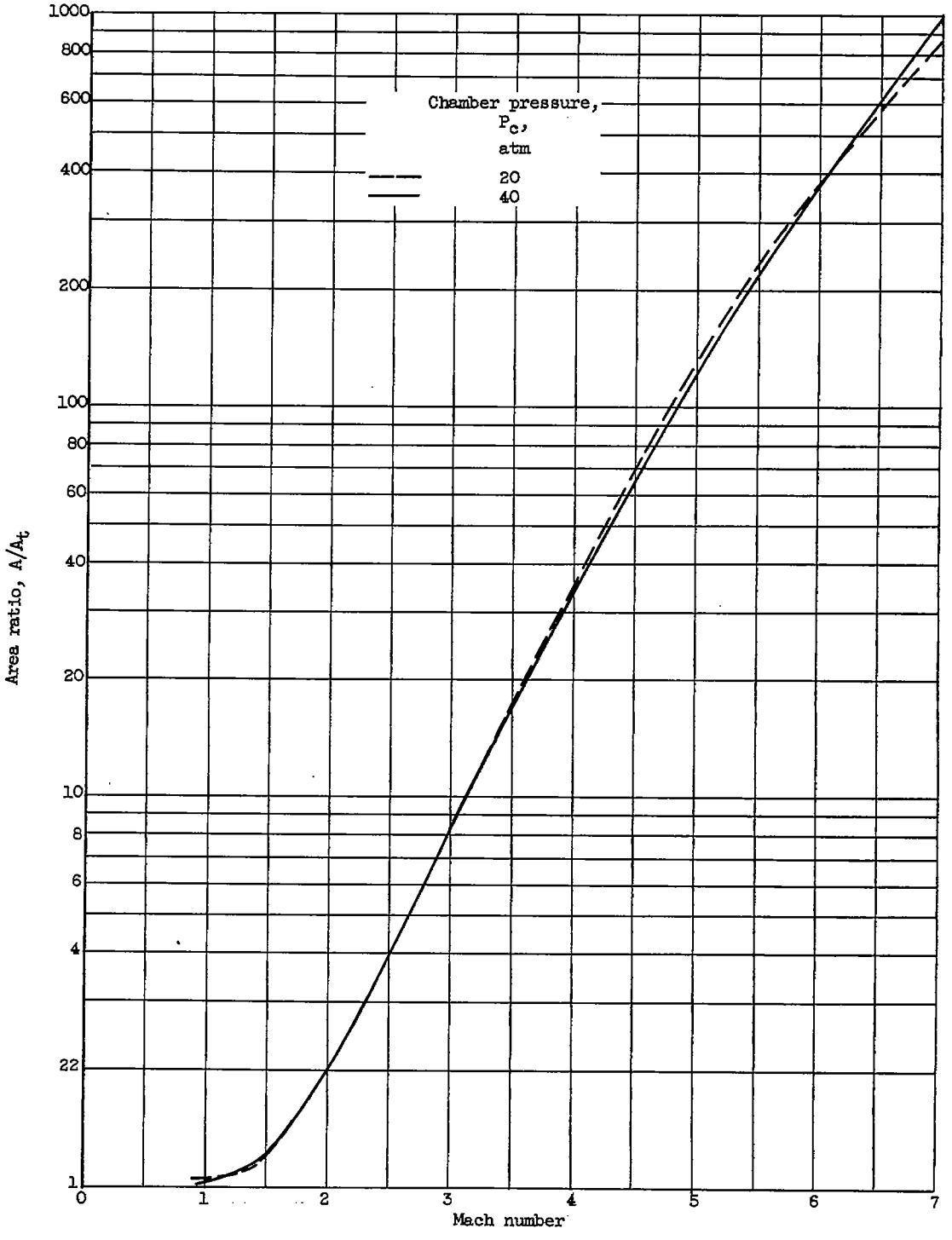

(c) Stoichiometric mixture.

Figure 8. - Concluded. Relation of one-dimensional area ratio and Mach number for ammonia-oxygen combustion gases.

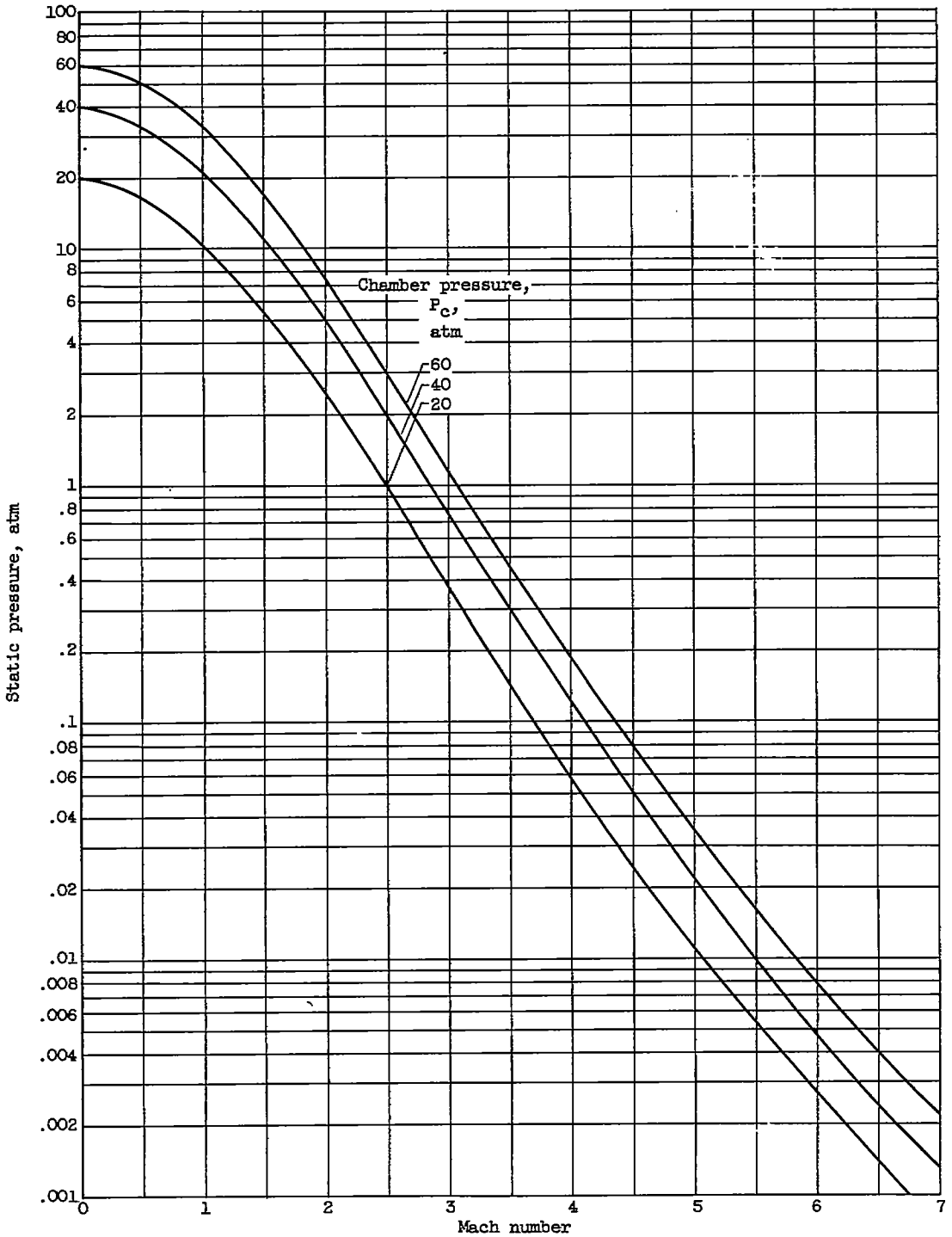

(a) Excess oxygen, 20 percent.

Figure 9. - Relation of one-dimensional static pressure and Mach number for ammonia-oxygen combustion gases.

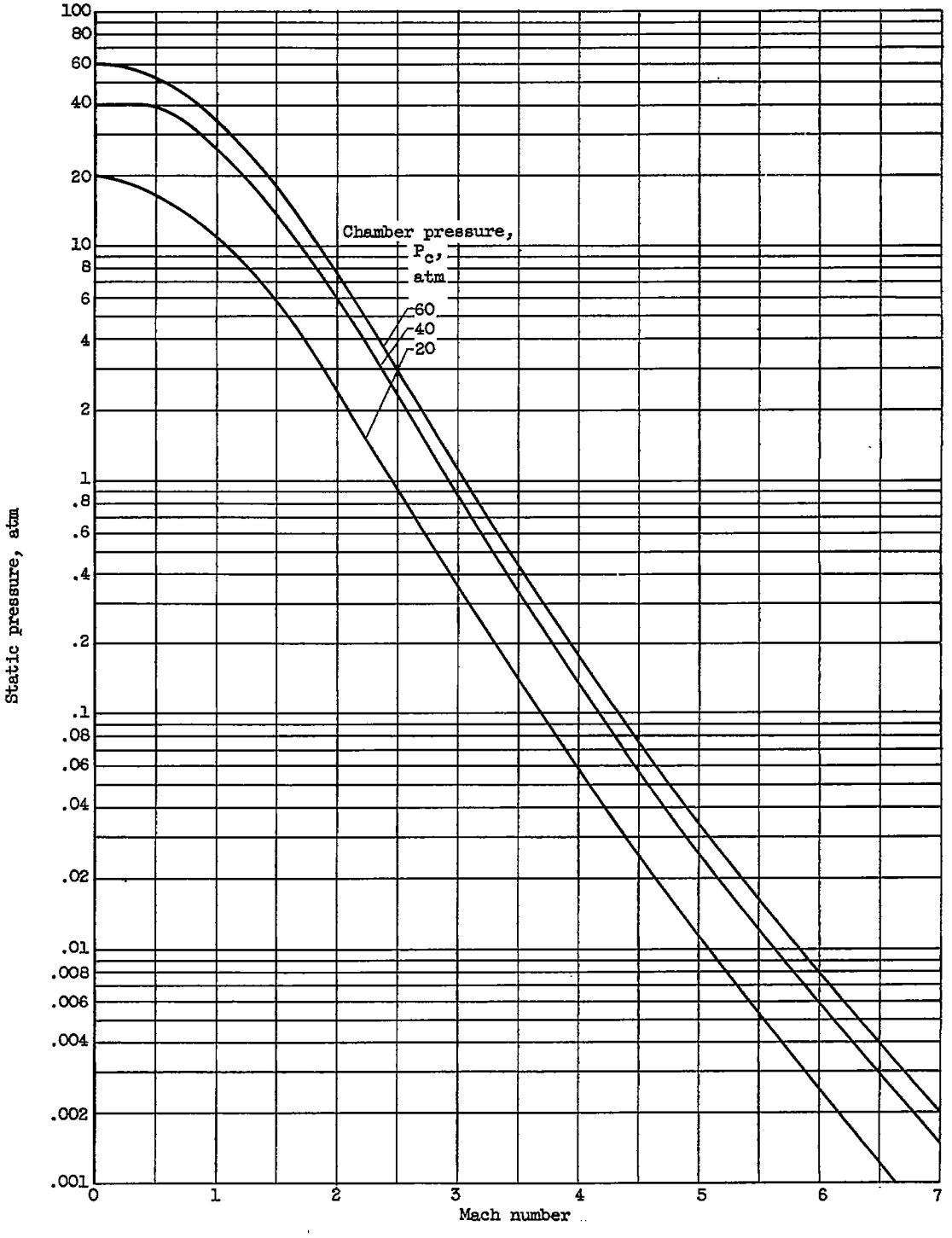

(b) Excess oxygen, 10 percent.

Figure 9. - Continued. Relation of one-dimensional static pressure and Mach number for ammonia-oxygen combustion gases.

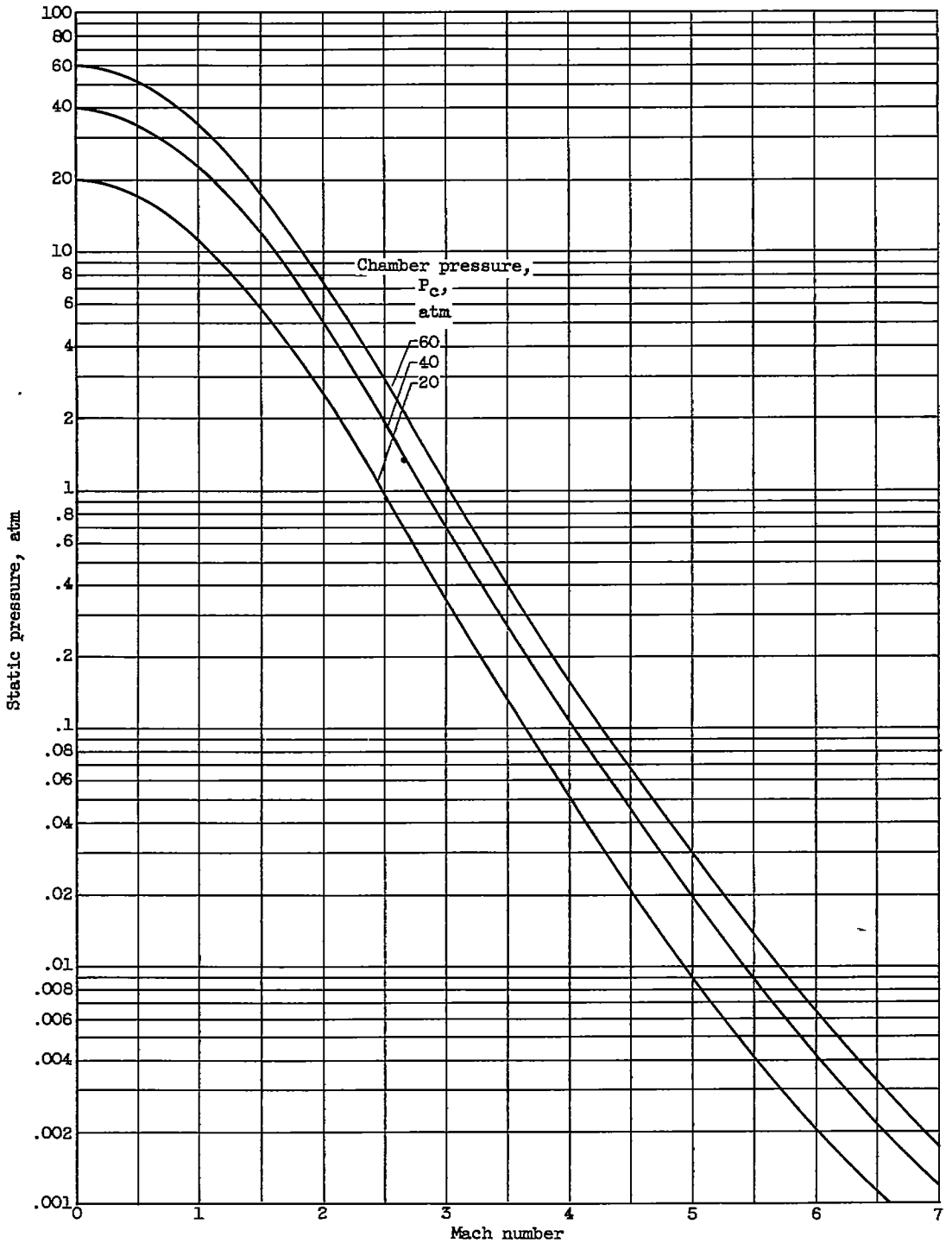

(c) Stoichiometric mixture.

Figure 9. - Concluded. Relation of one dimensional static pressure and Mach number for ammonia-oxygen combustion gases.

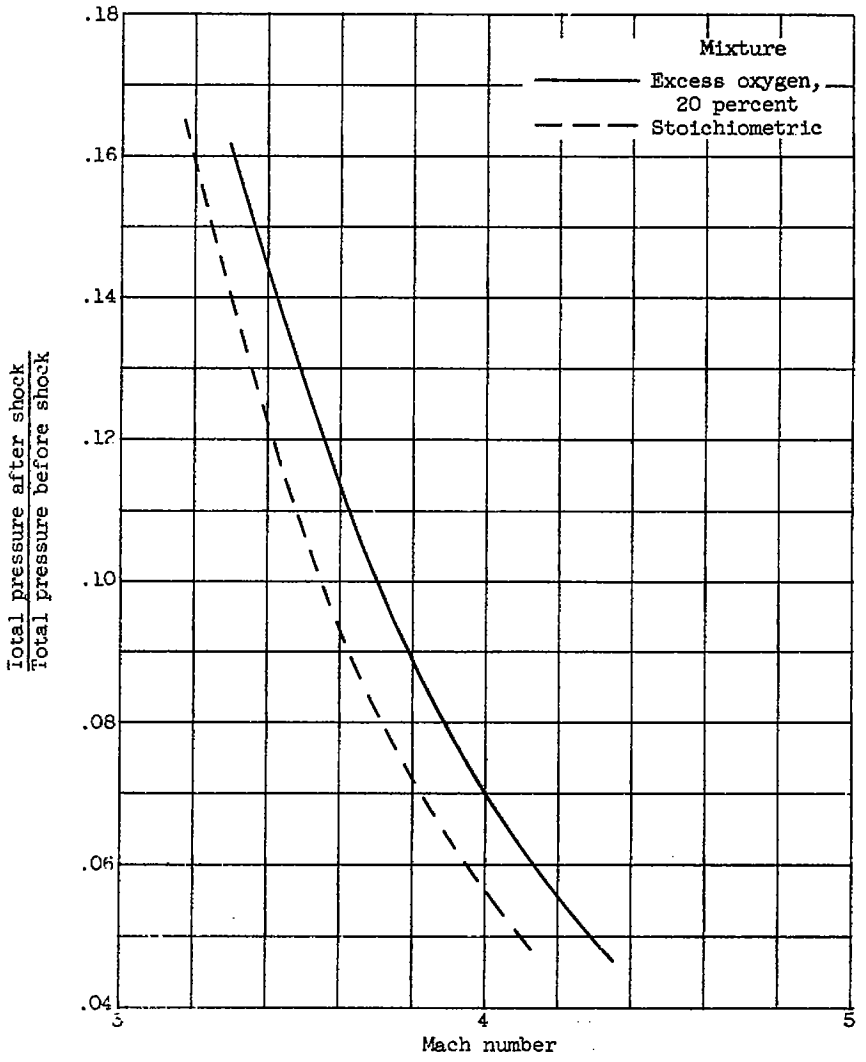

Figure 10. - Pressure ratio across normal shock for combustion products of ammonia and oxygen. Upstream total pressure, 40 atmospheres.

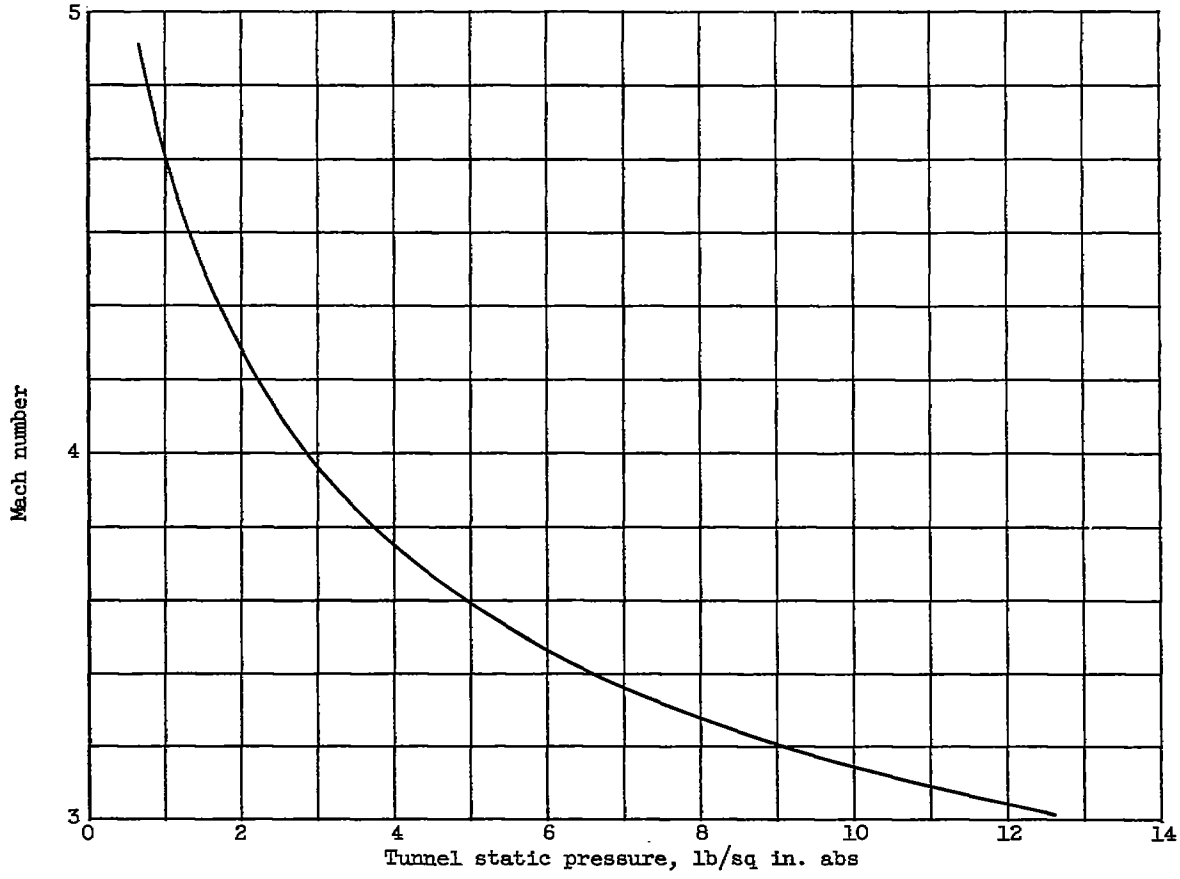

Figure 11. - Tunnel Mach number as function of static pressure for incomplete combustion. Total pressure, 600 pounds per square inch absolute; combustion efficiency, 90 percent.

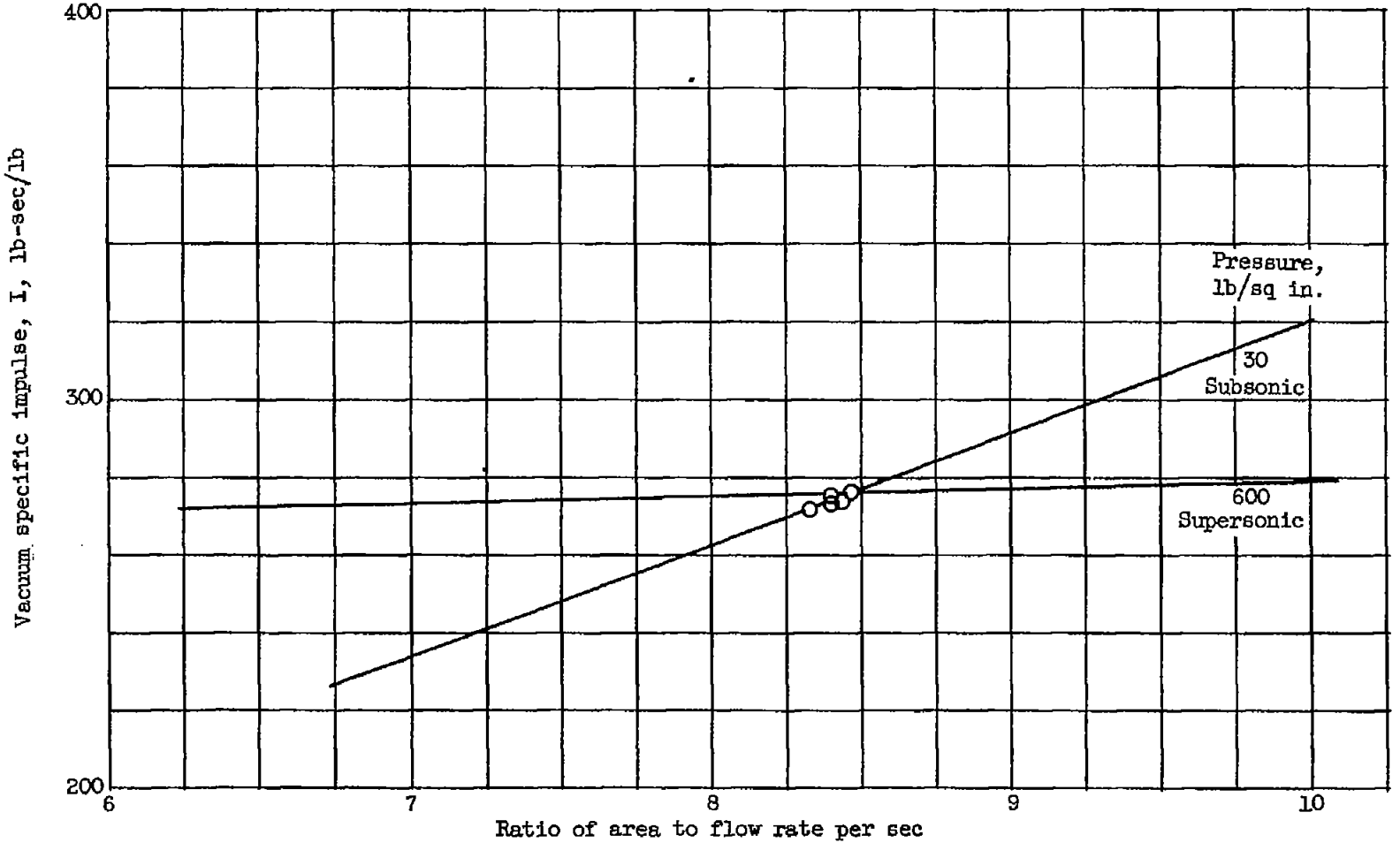

Figure 12. - Constant momentum solution across normal shock for ammonia, oxygen, and nitrogen system. Combustion efficiency, 90 percent.

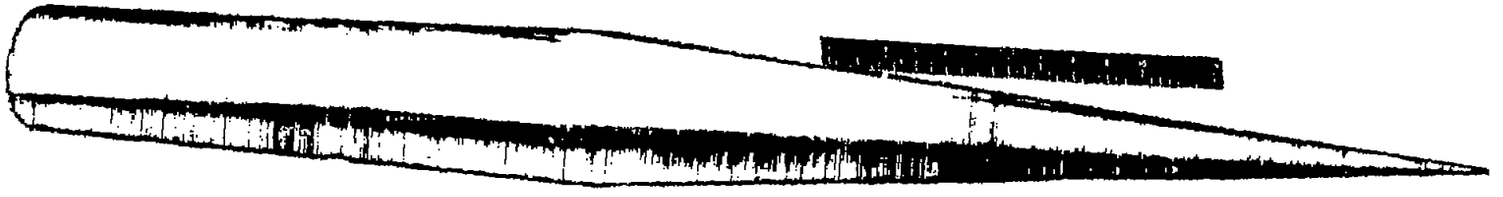

CS-15314

Figure 13. - Heat-transfer model.

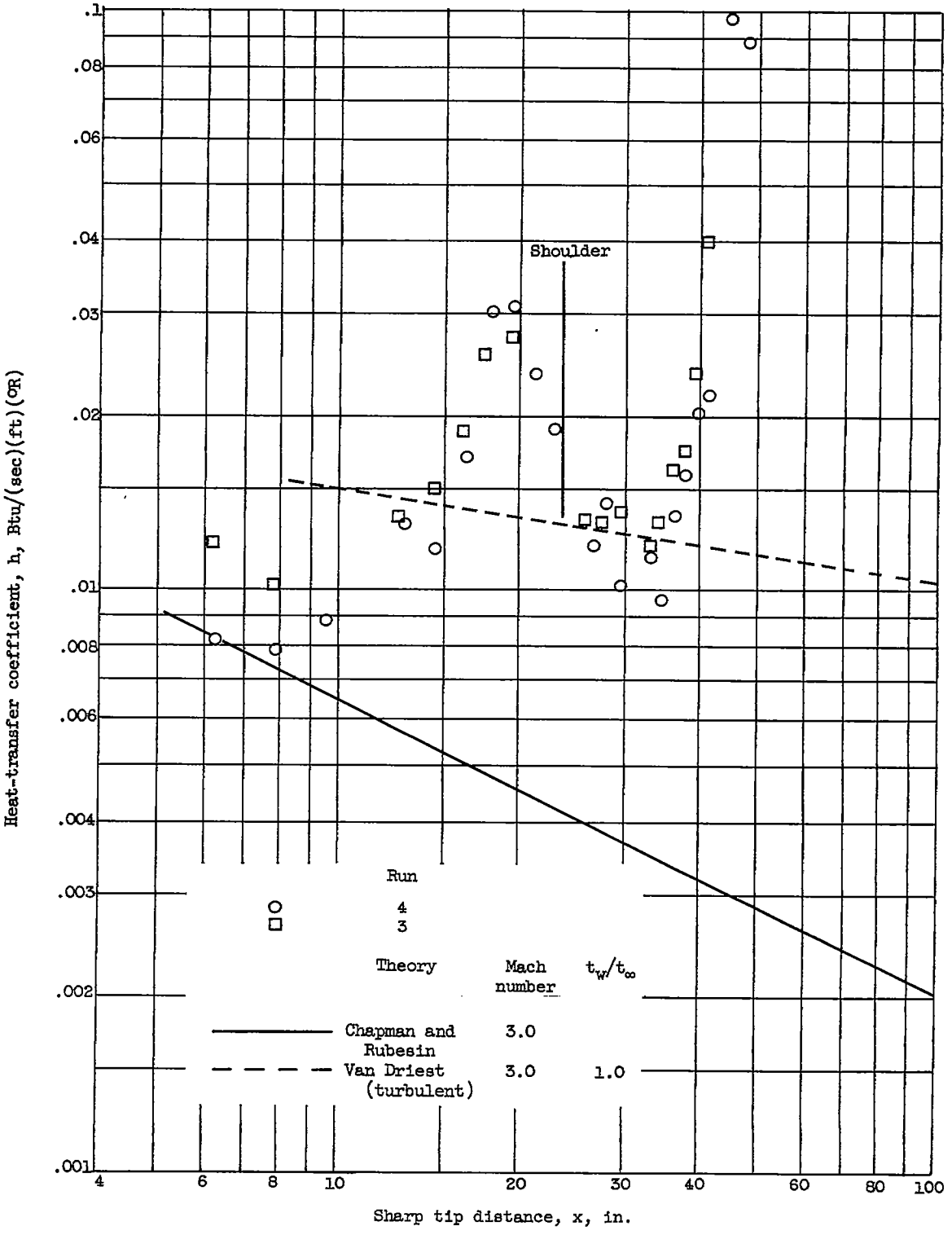

Figure 14. - Heat-transfer coefficient profile on model.

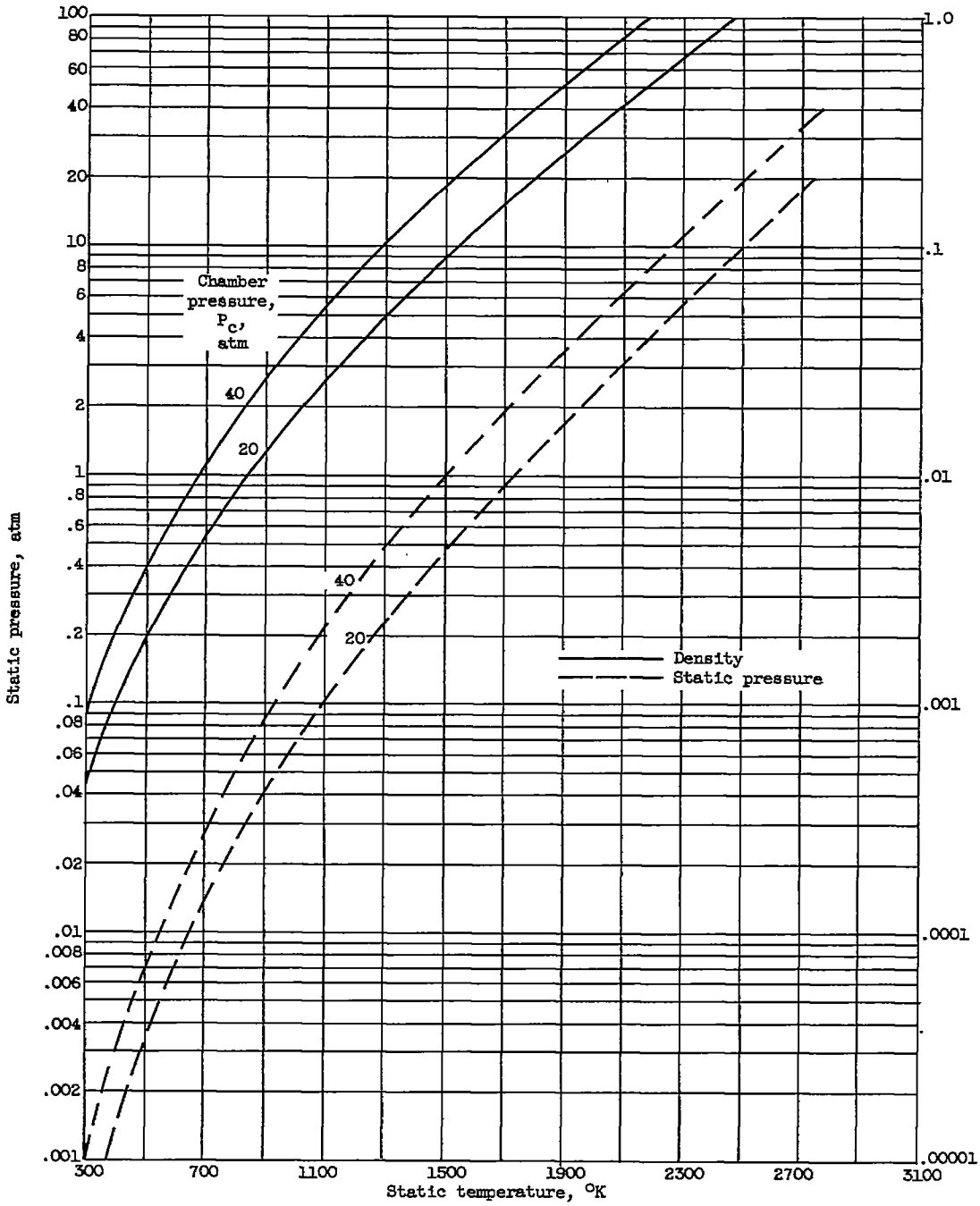

(a) Excess oxygen, 20 percent.

Figure 15. - Static pressure, density, and temperature relations for ammonia-oxygen combustion products.

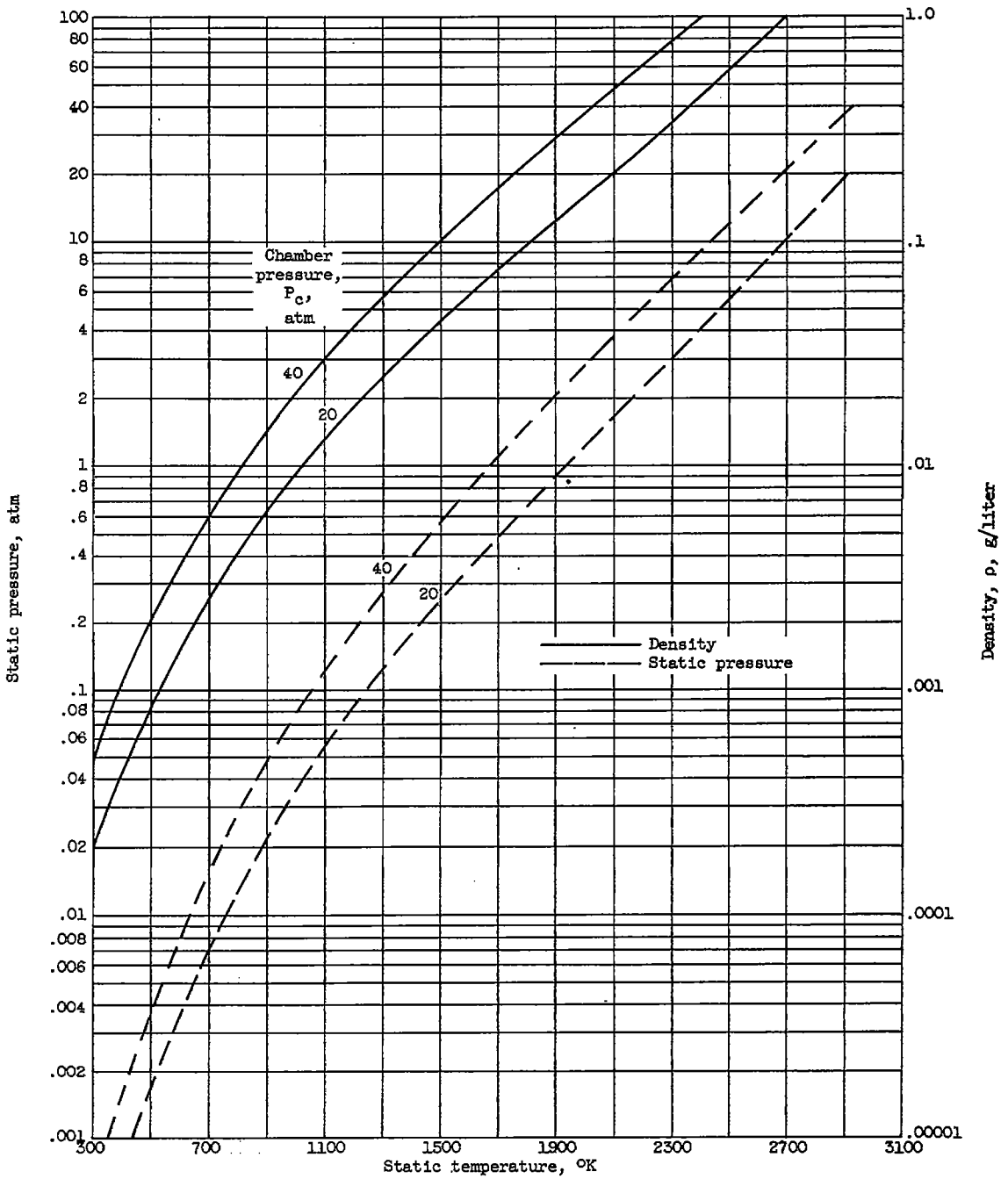

(b) Excess oxygen, 10 percent.

Figure 15. - Continued. Static pressure density, and temperature relations for ammonia-oxygen combustion products.

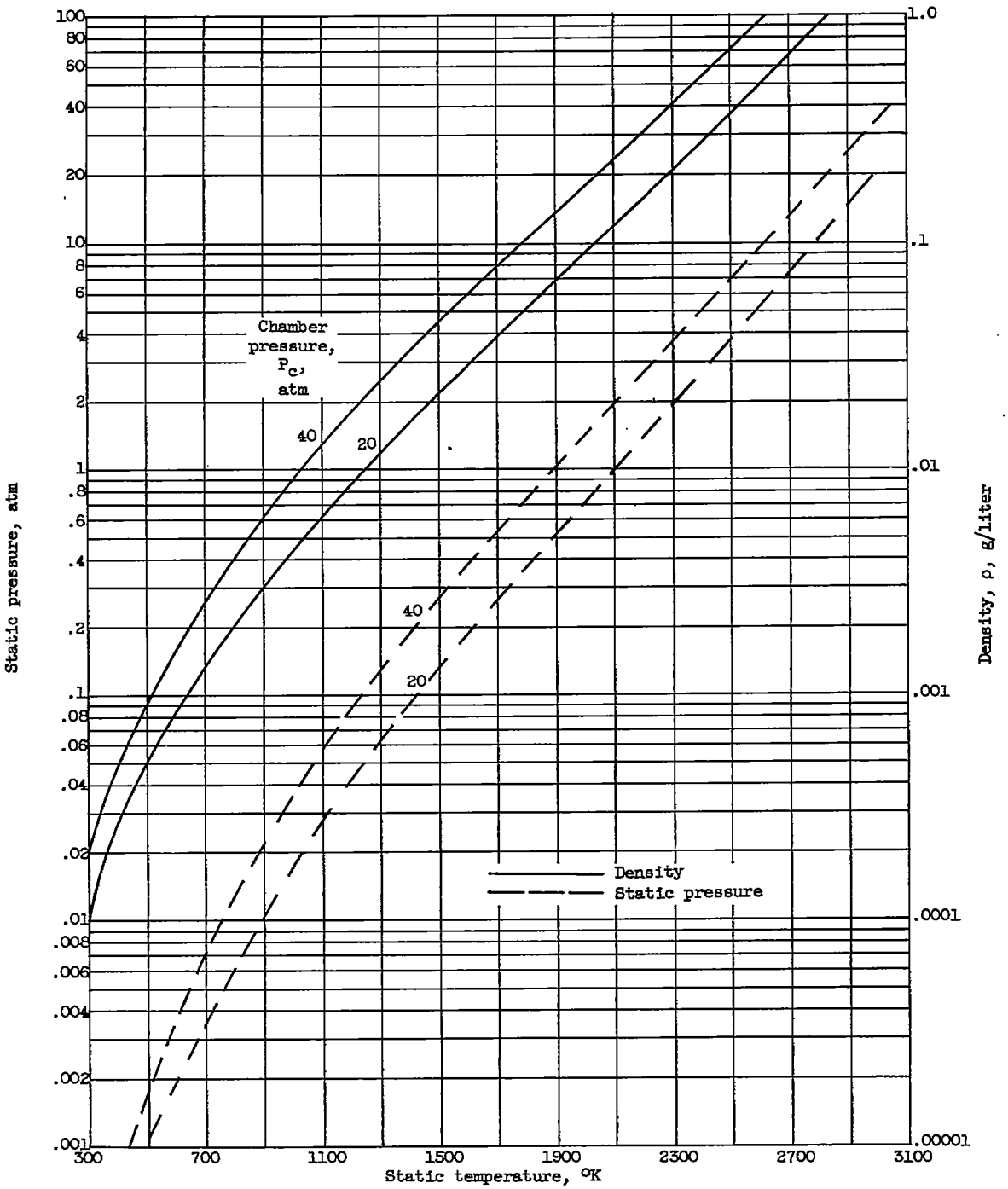

(c) Stoichiometric conditions.

Figure 15. - Concluded. Static pressure, density, and temperature relations for ammonia-oxygen combustion products.

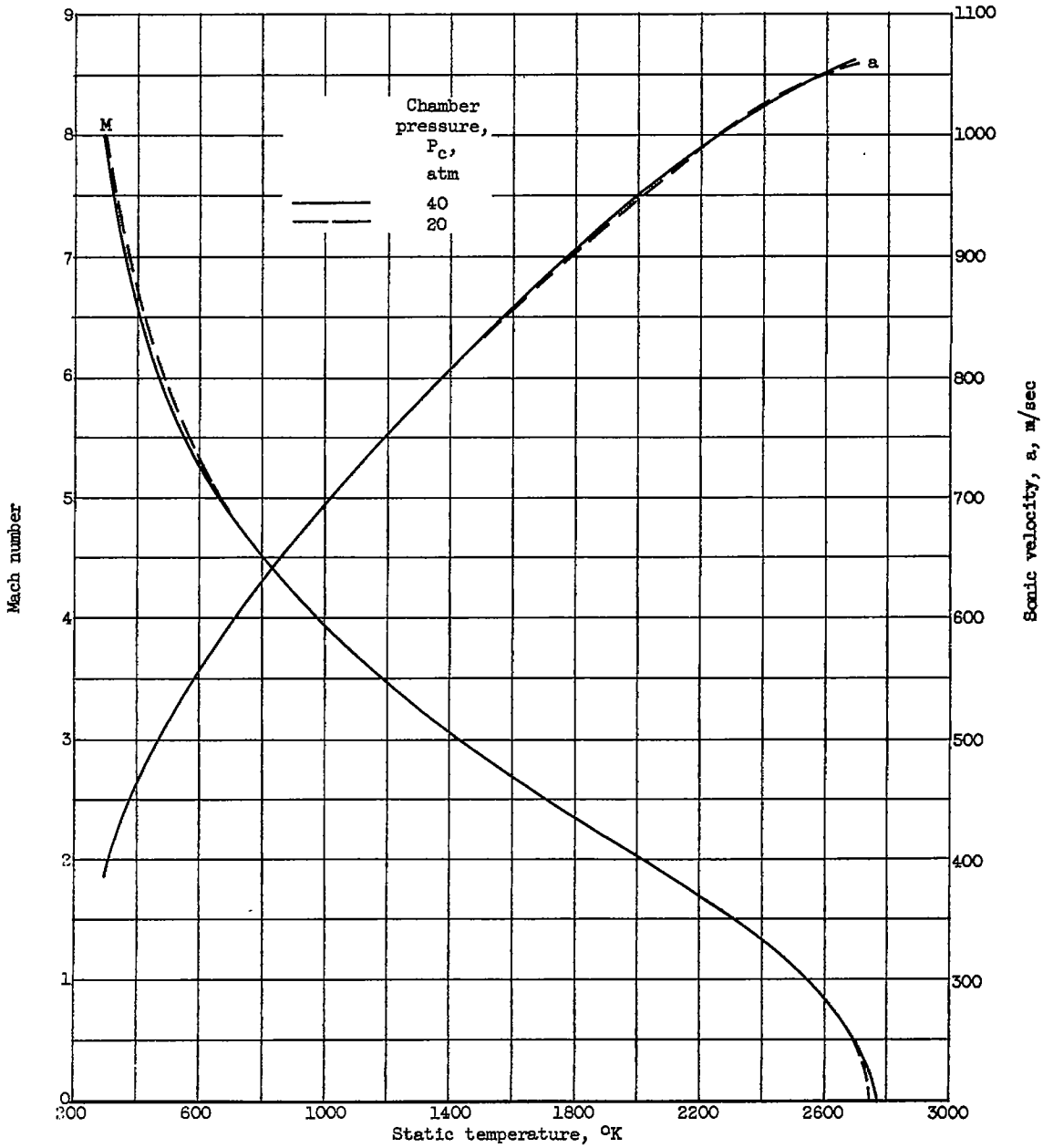

(a) Excess oxygen, 20 percent.

Figure 16. - Sonic velocity and Mach number as function of static temperature for ammonia-oxygen combustion products.

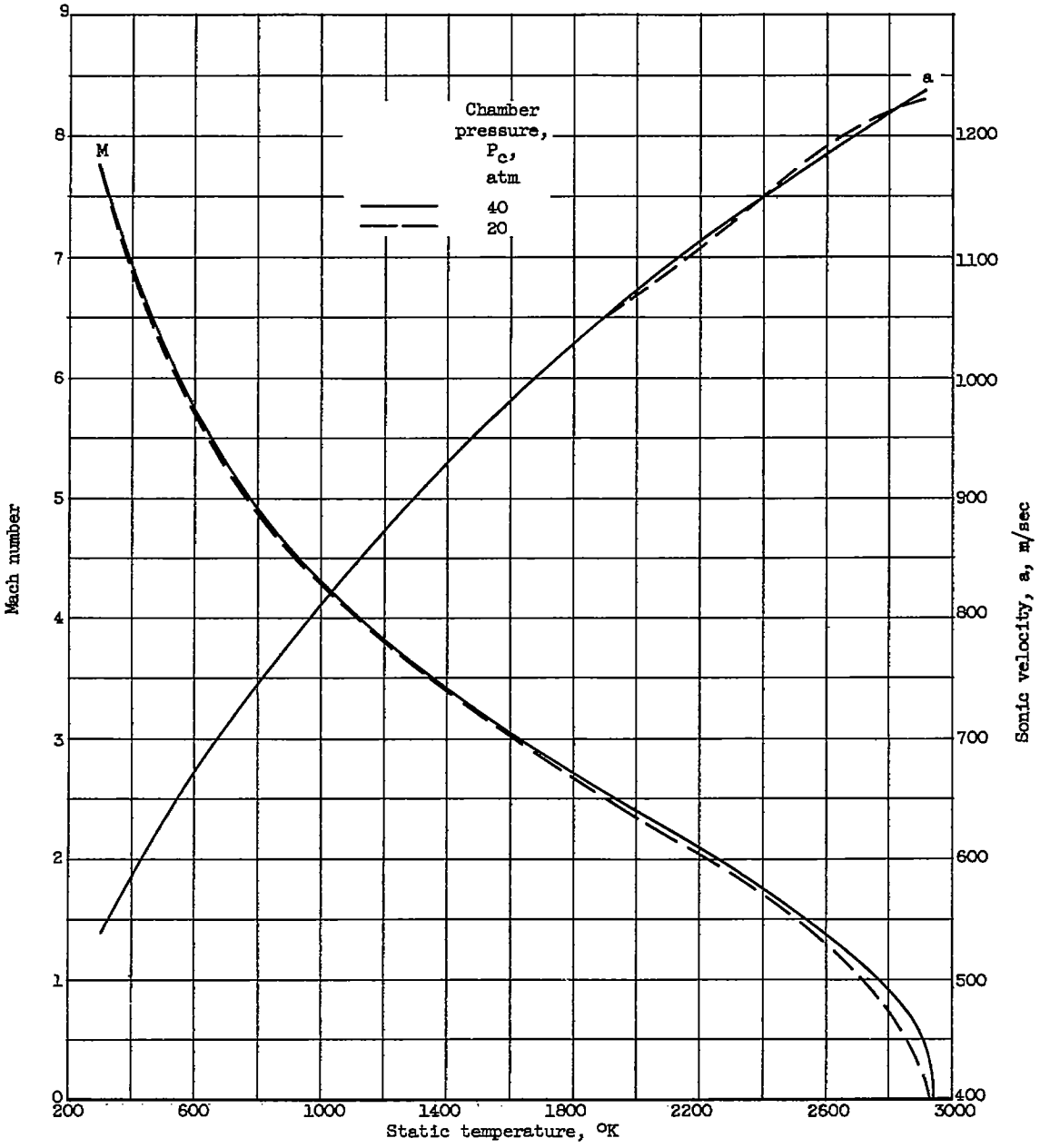

(b) Excess oxygen, 10 percent.

Figure 16. - Continued. Sonic velocity and Mach number as function of static temperature for ammonia-oxygen combustion products.

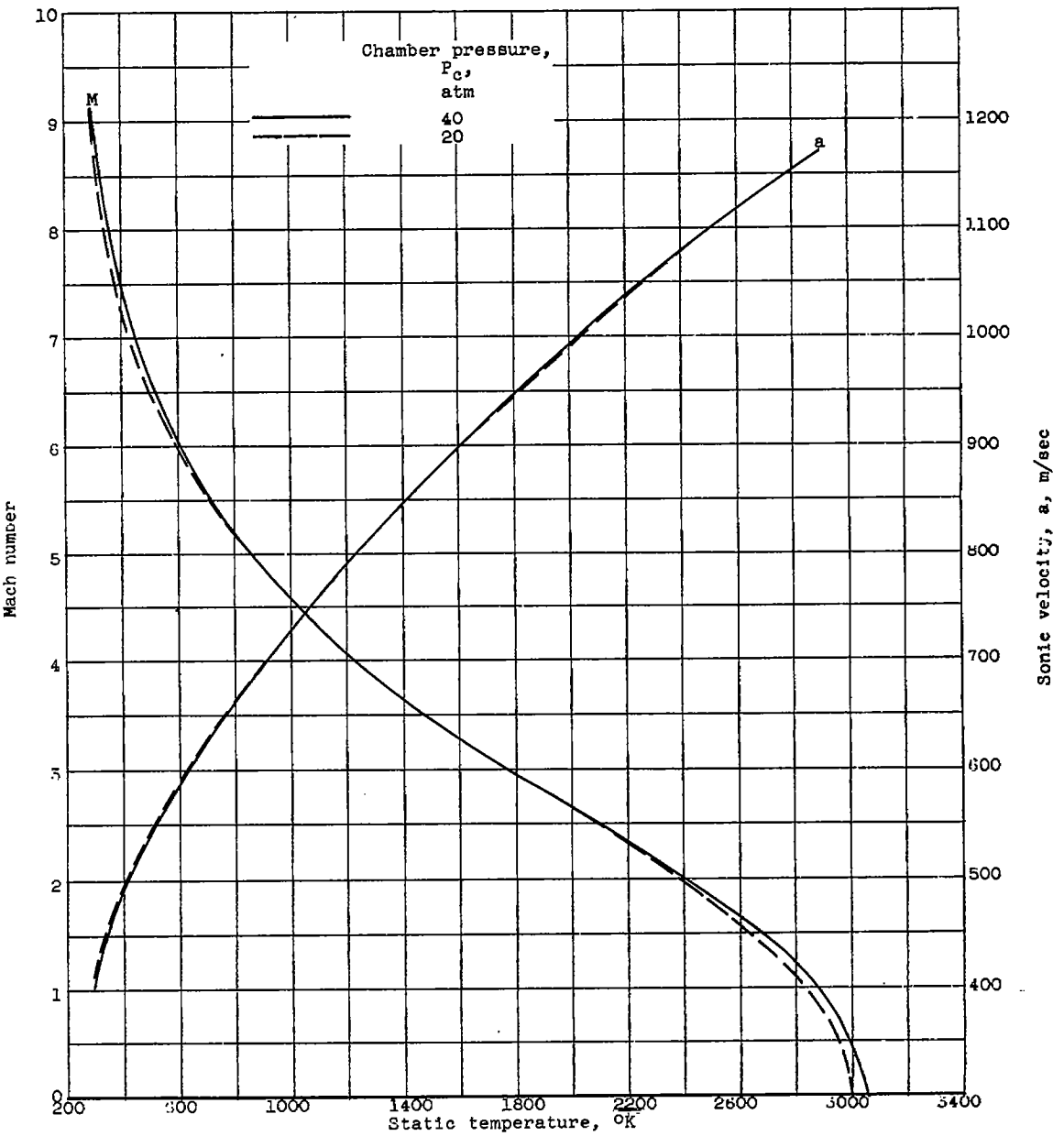

(c) Stoichiometric mixture.

Figure 16. - Concluded. Sonic velocity and Mach number as function of static temperature for ammonia-oxygen combustion products. Stoichiometric mixture.

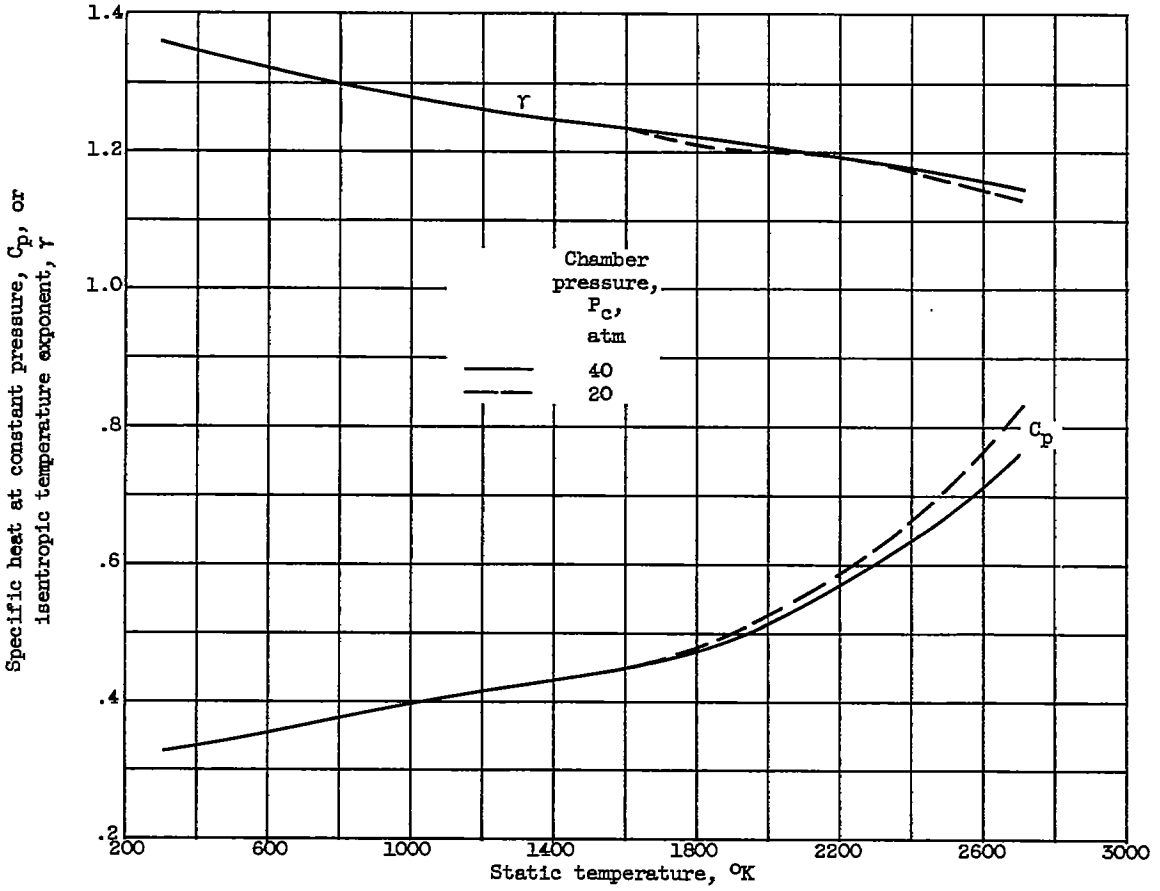

(a) Excess oxygen, 20 percent.

Figure 17. - Specific heat data over a range of static temperatures for ammonia-oxygen combustion products.

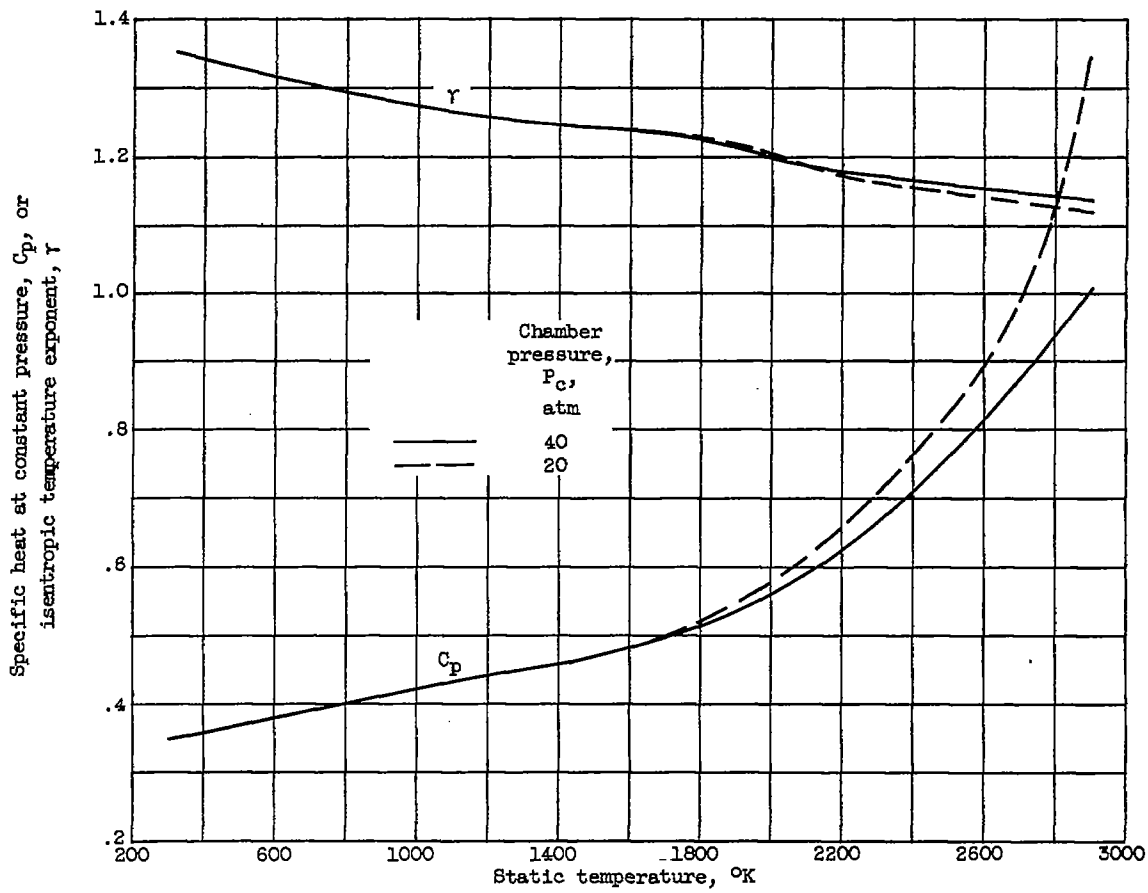

(b) Excess oxygen, 10 percent.

Figure 17. - Continued. Specific heat data over a range of static temperatures for ammonia-oxygen combustion products.

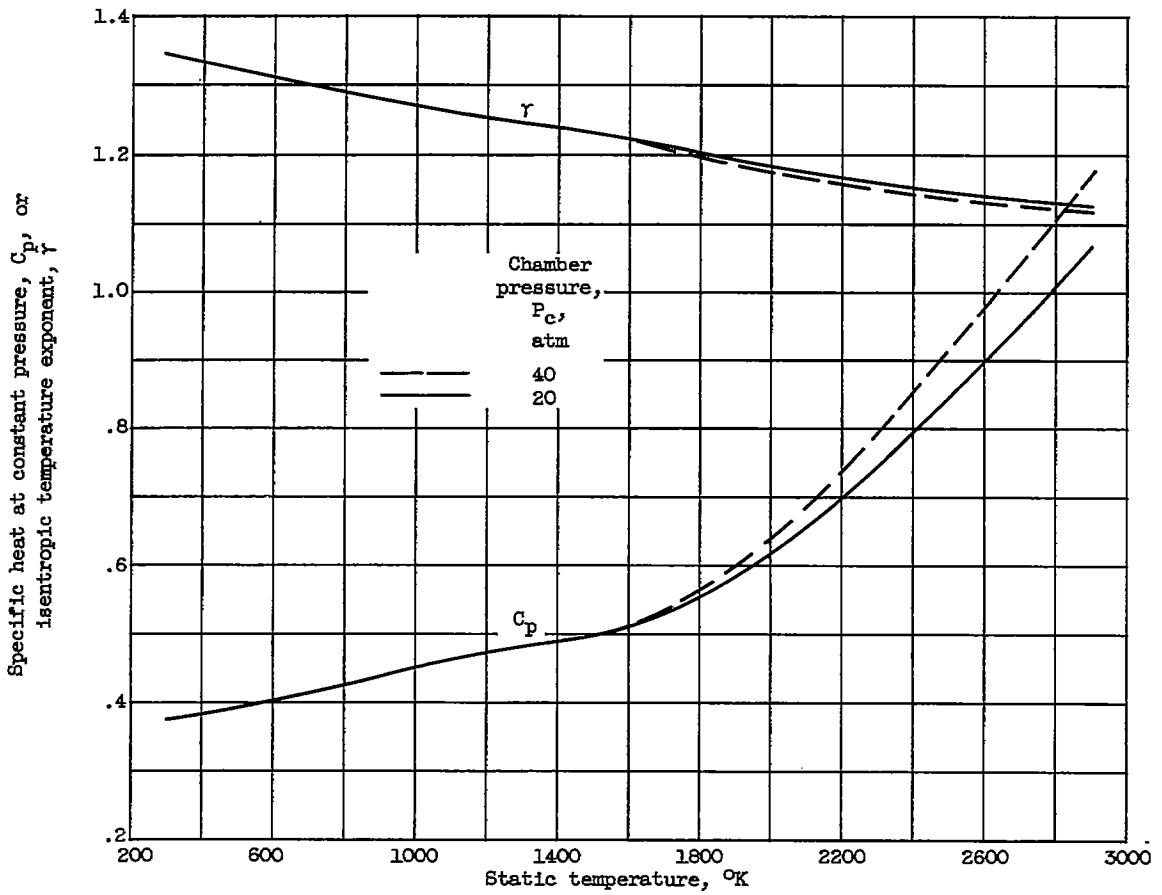

(c) Stoichiometric conditions.

Figure 17. - Concluded. Specific heat data over a range of static temperatures for ammonia-oxygen combustion products.

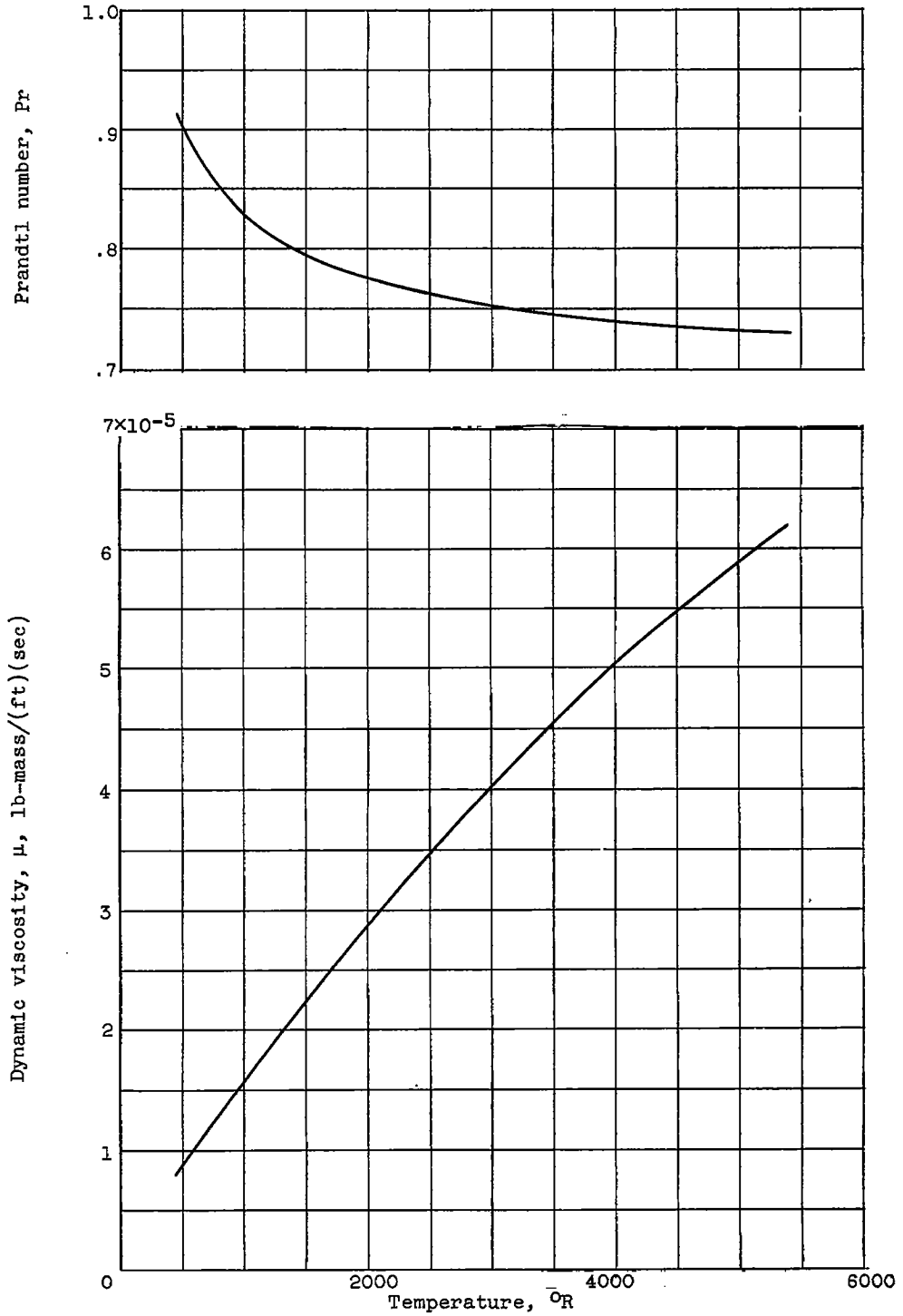

(a) Excess oxygen, 20 percent.

Figure 18. - Transport data for products of combustion of ammonia and oxygen.

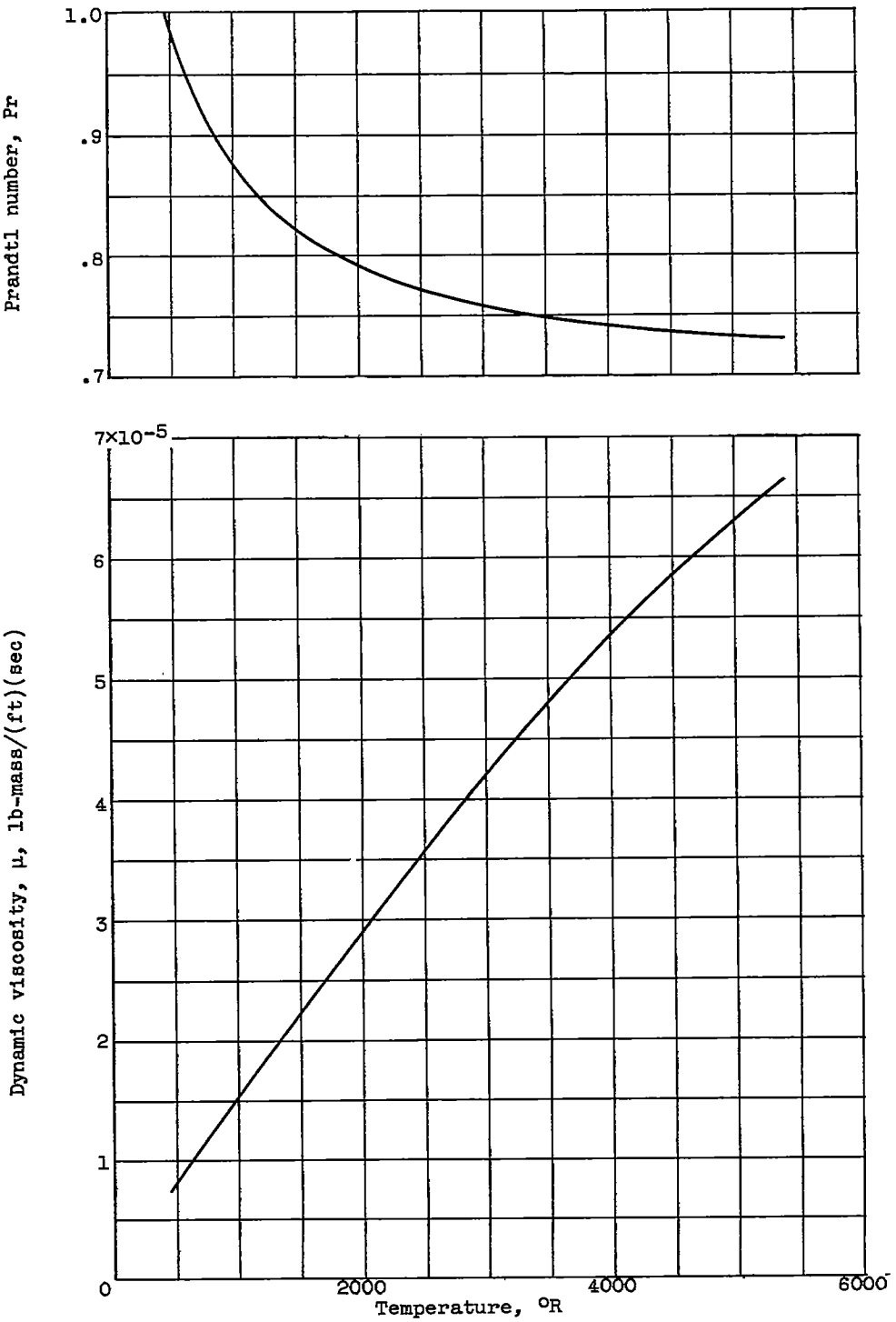

(b) Stoichiometric conditions.

Figure 18. - Concluded. Transport data for products of combustion of ammonia and oxygen.

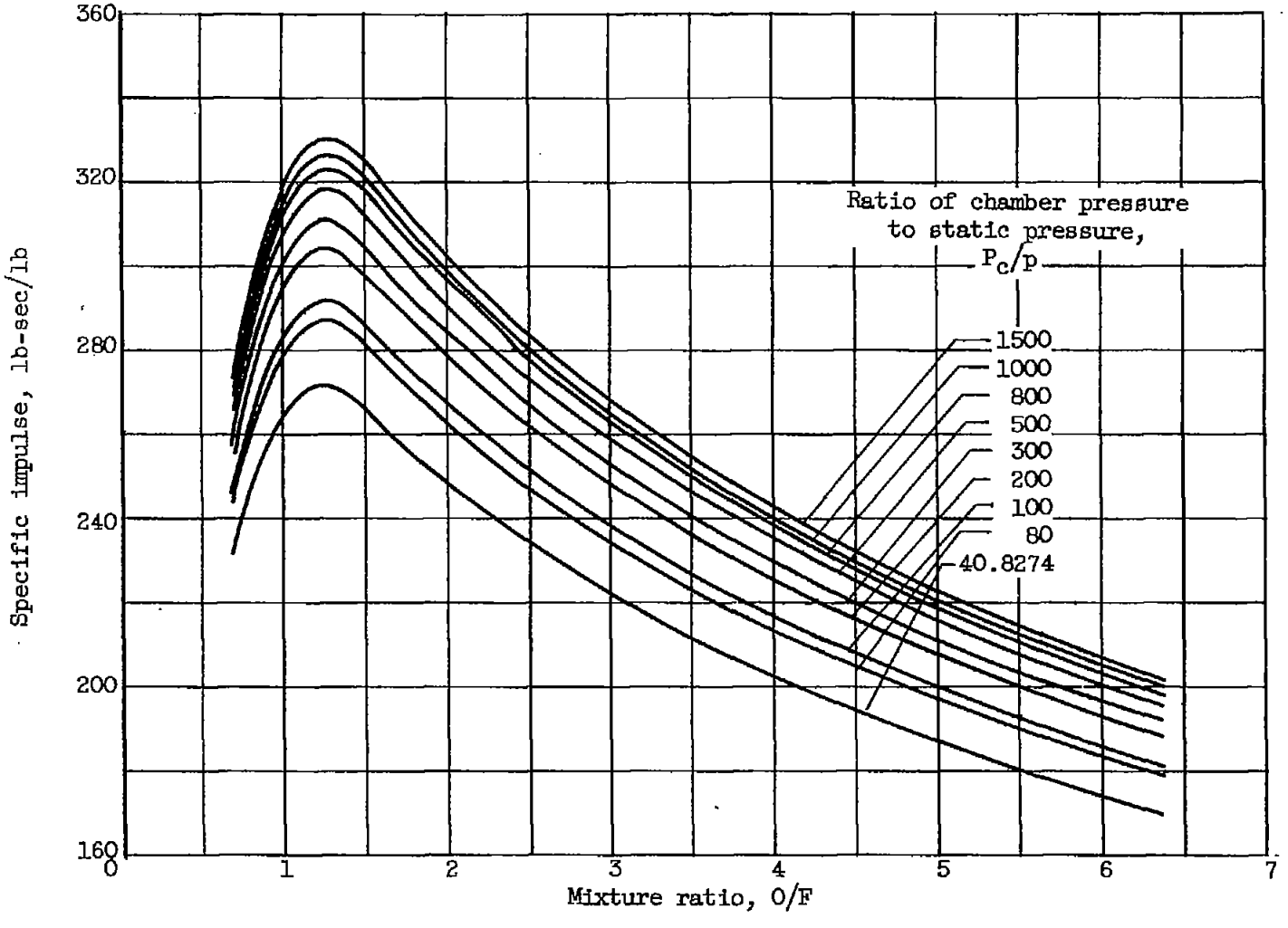

(a) Frozen properties.

Figure 19. - Specific impulse of ammonia and oxygen. Static chamber pressure, 600 pounds per square inch absolute.

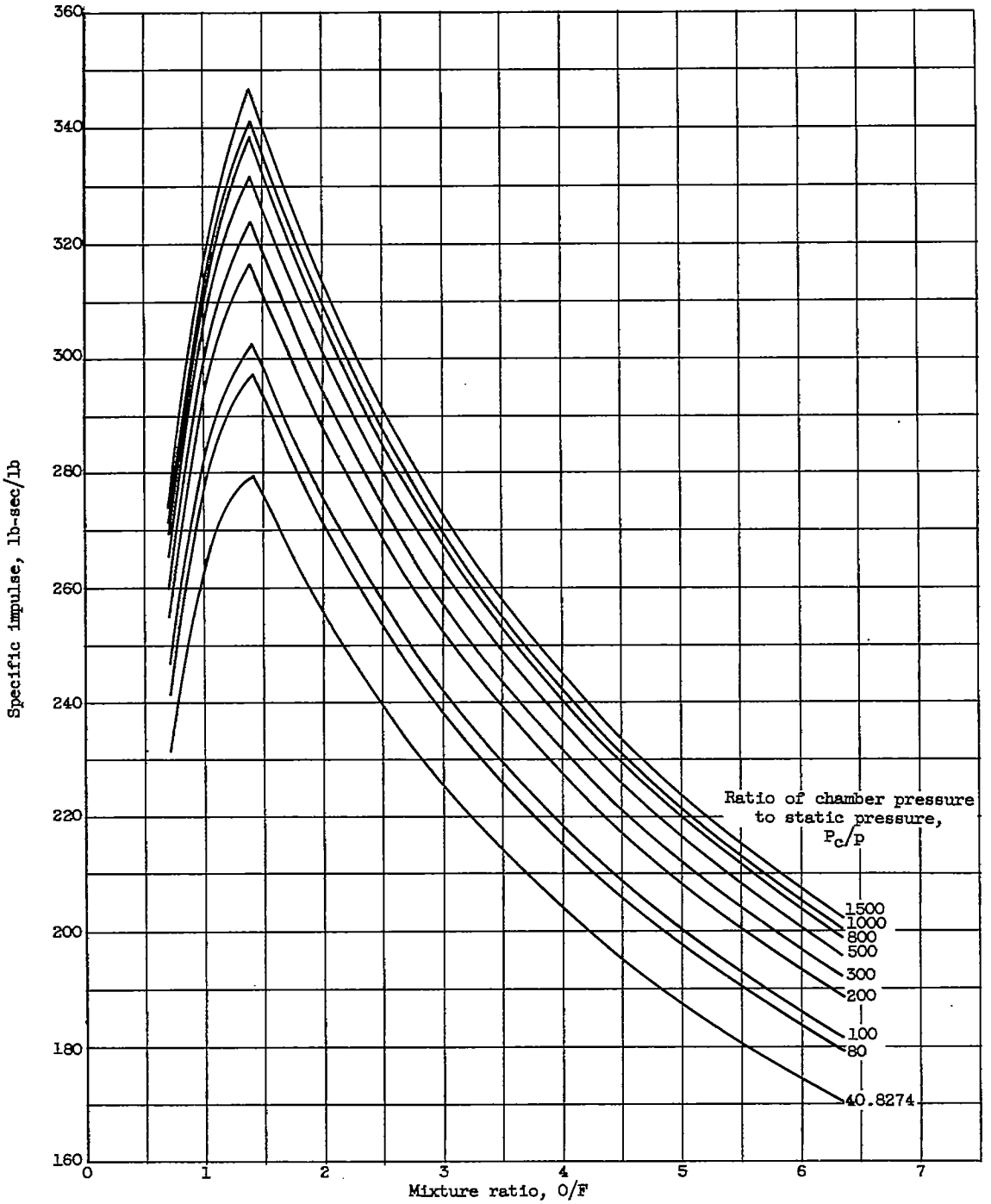

(b) Chemical equilibrium.

Figure 19. - Concluded. Specific impulse of ammonia-oxygen. Static chamber pressure, 600 pounds per square inch absolute.

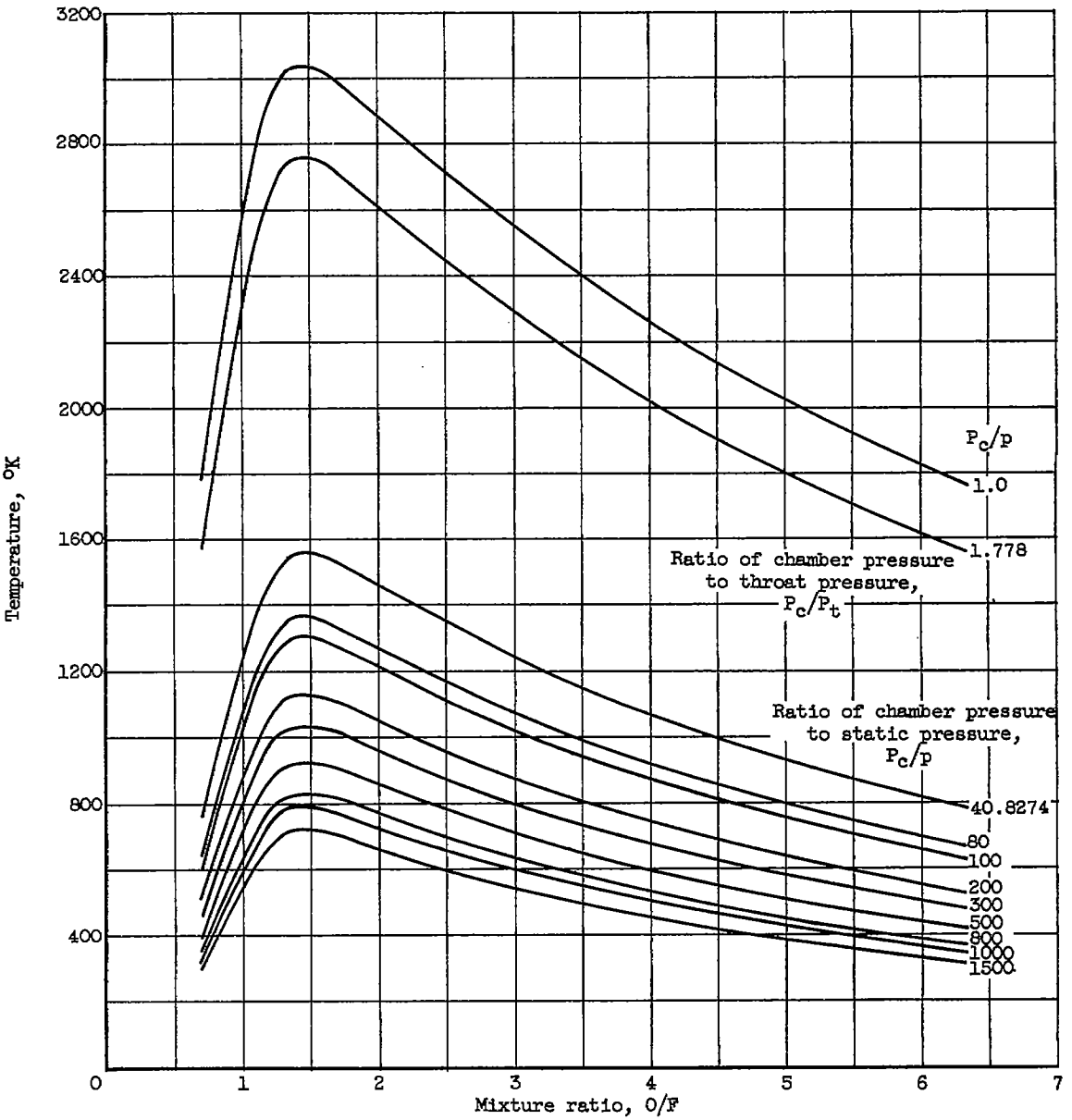

(a) Frozen conditions.

Figure 20. - Combustion temperature of ammonia and oxygen over a range of mixture ratios.

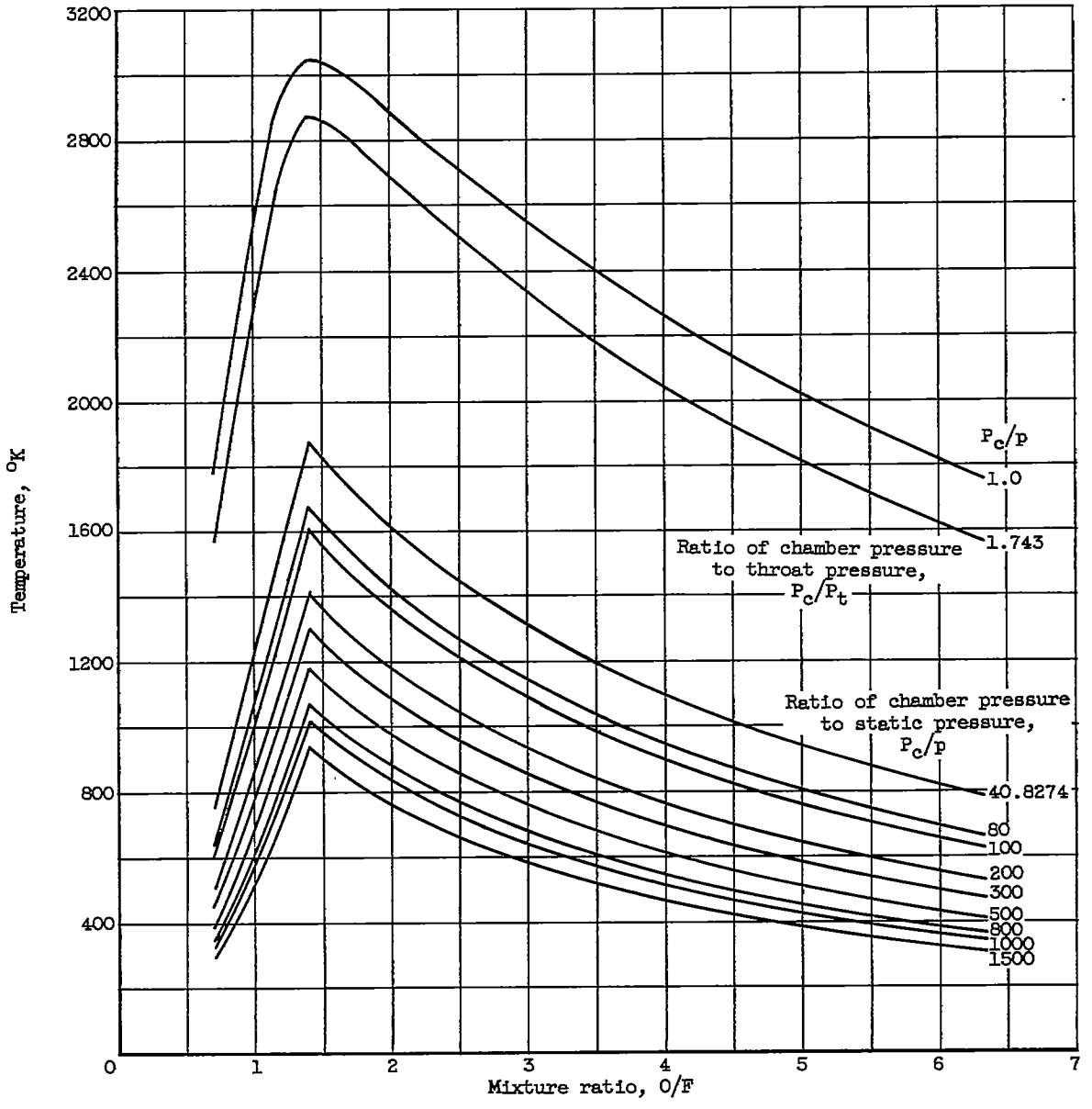

(b) Chemical equilibrium.

Figure 20. - Concluded. Combustion temperature of ammonia and oxygen over a range of mixture ratios.

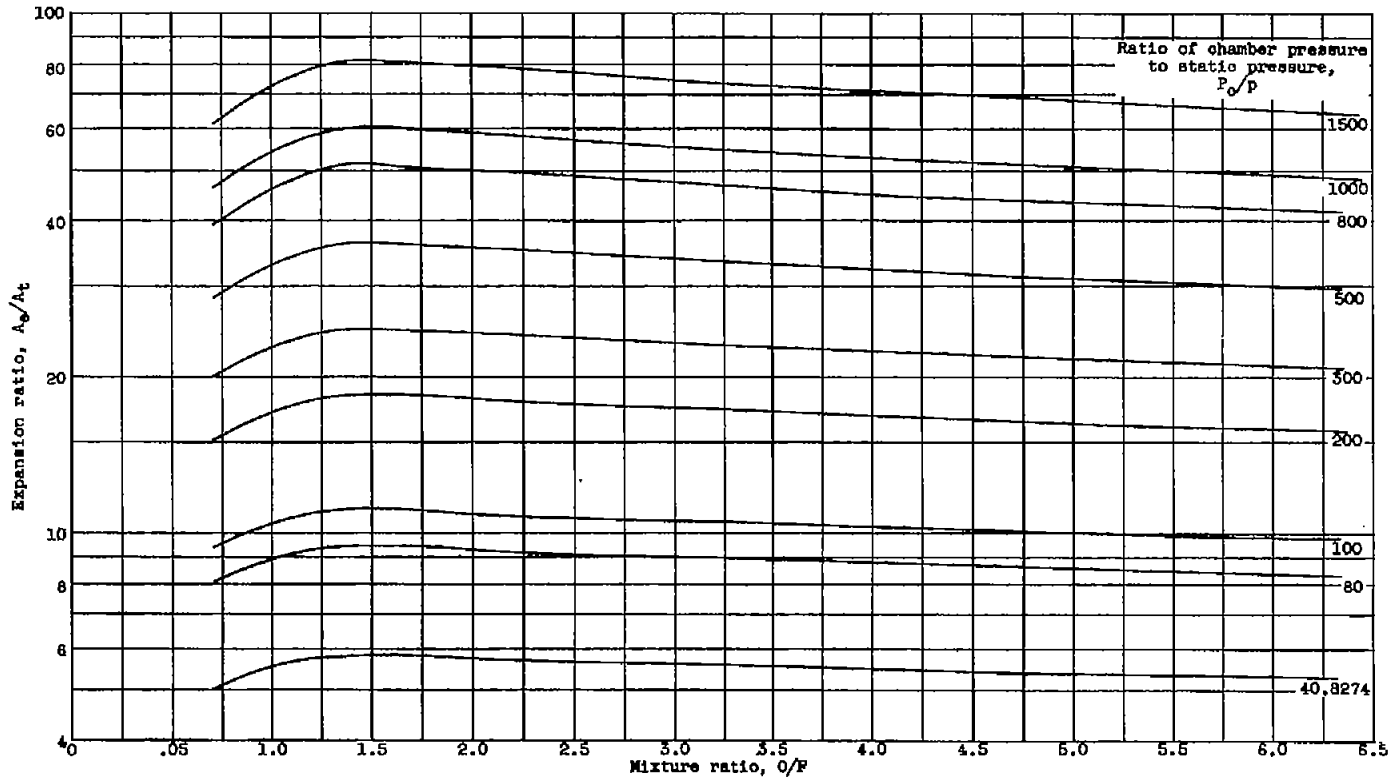

(a) Frozen properties.

Figure 21. - Area ratio as a function of mixture ratio data for ammonia and oxygen.

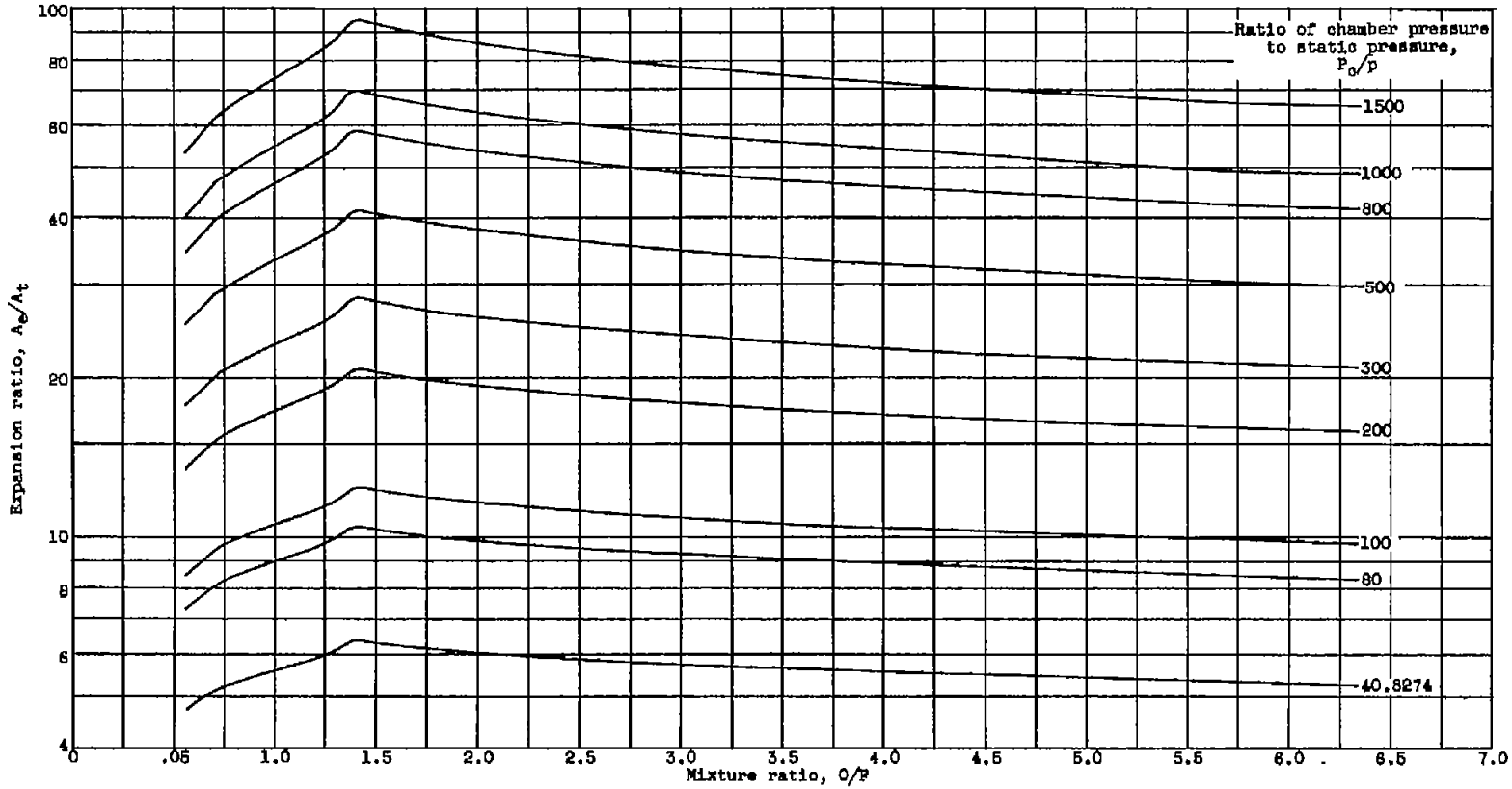

(b) Equilibrium conditions.

Figure 21. - Concluded. Area ratio as a function of mixture ratio data for ammonia and oxygen.

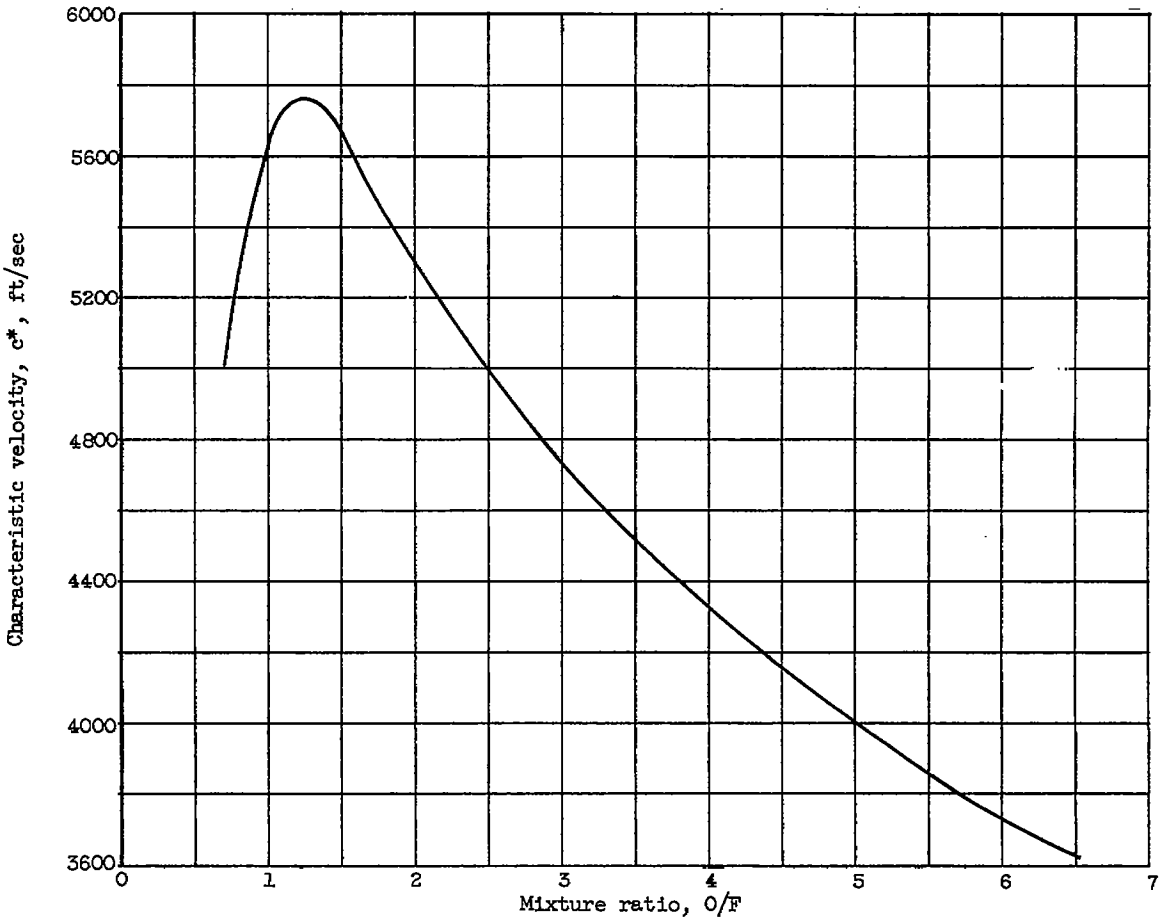

(a) Frozen conditions.

Figure 22. - Characteristic velocity as a function of mixture ratio for ammonia-oxygen combustion products.

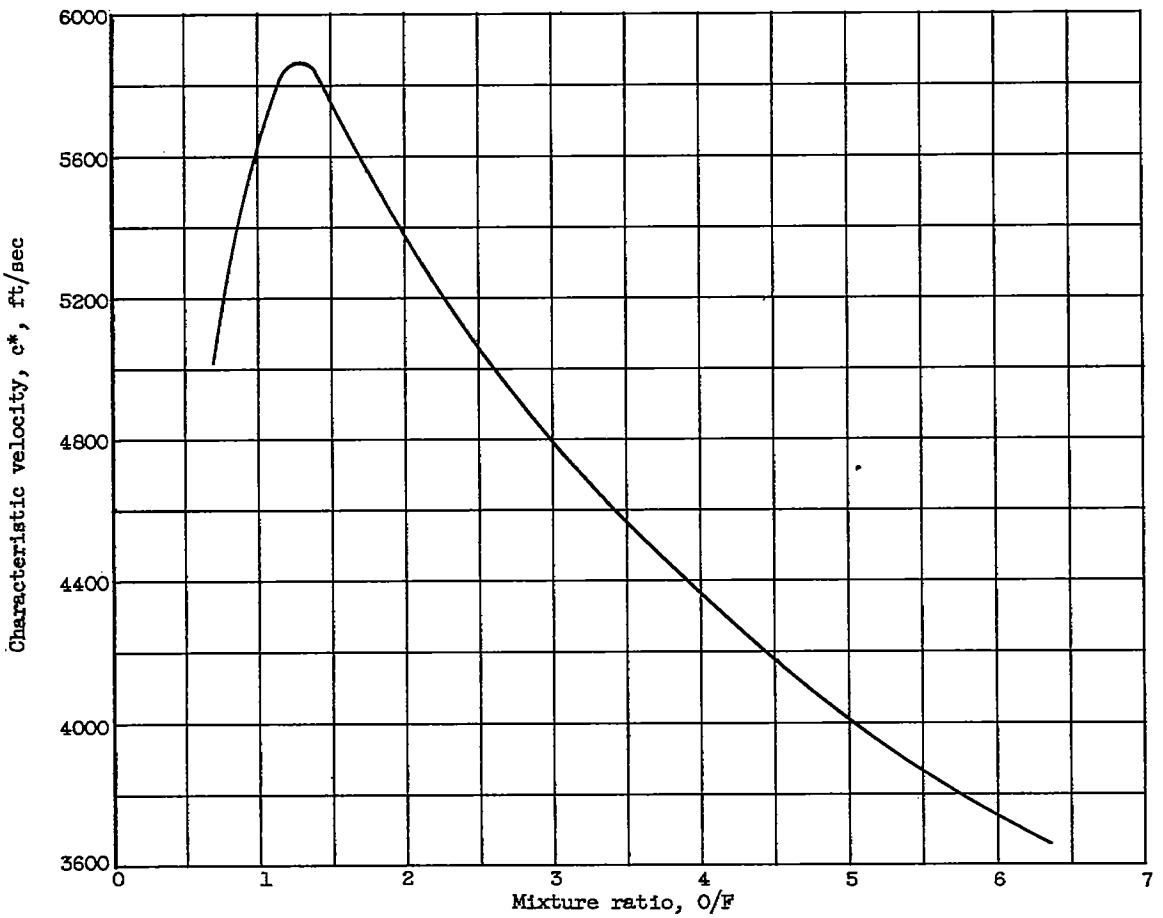

(b) Equilibrium conditions.

Figure 22. - Concluded. Characteristic velocity as a function of mixture ratio for ammonia-oxygen combustion products.

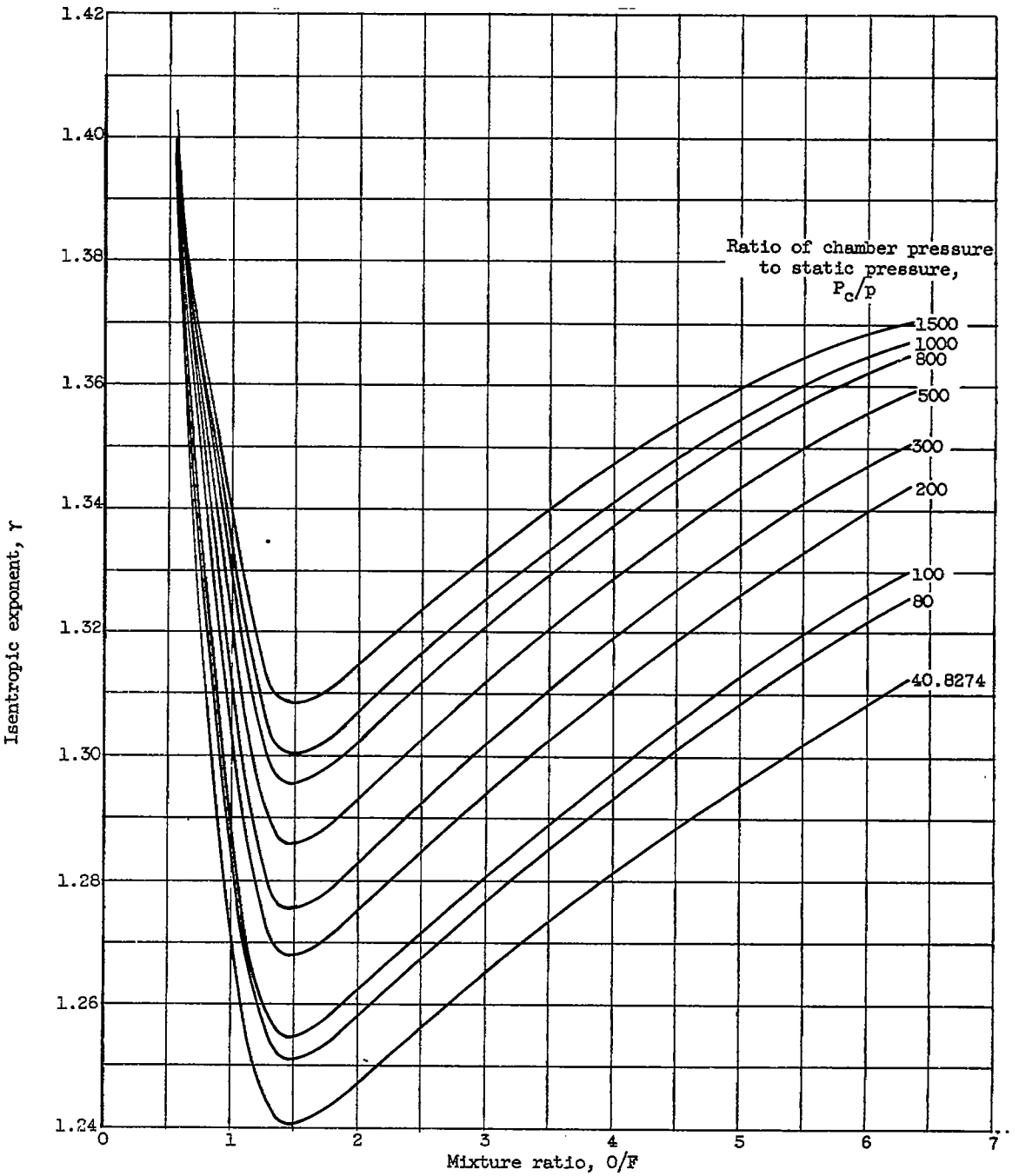

(a) Frozen conditions.

Figure 23. - Isentropic exponent as a function of mixture ratio for ammonia and oxygen.

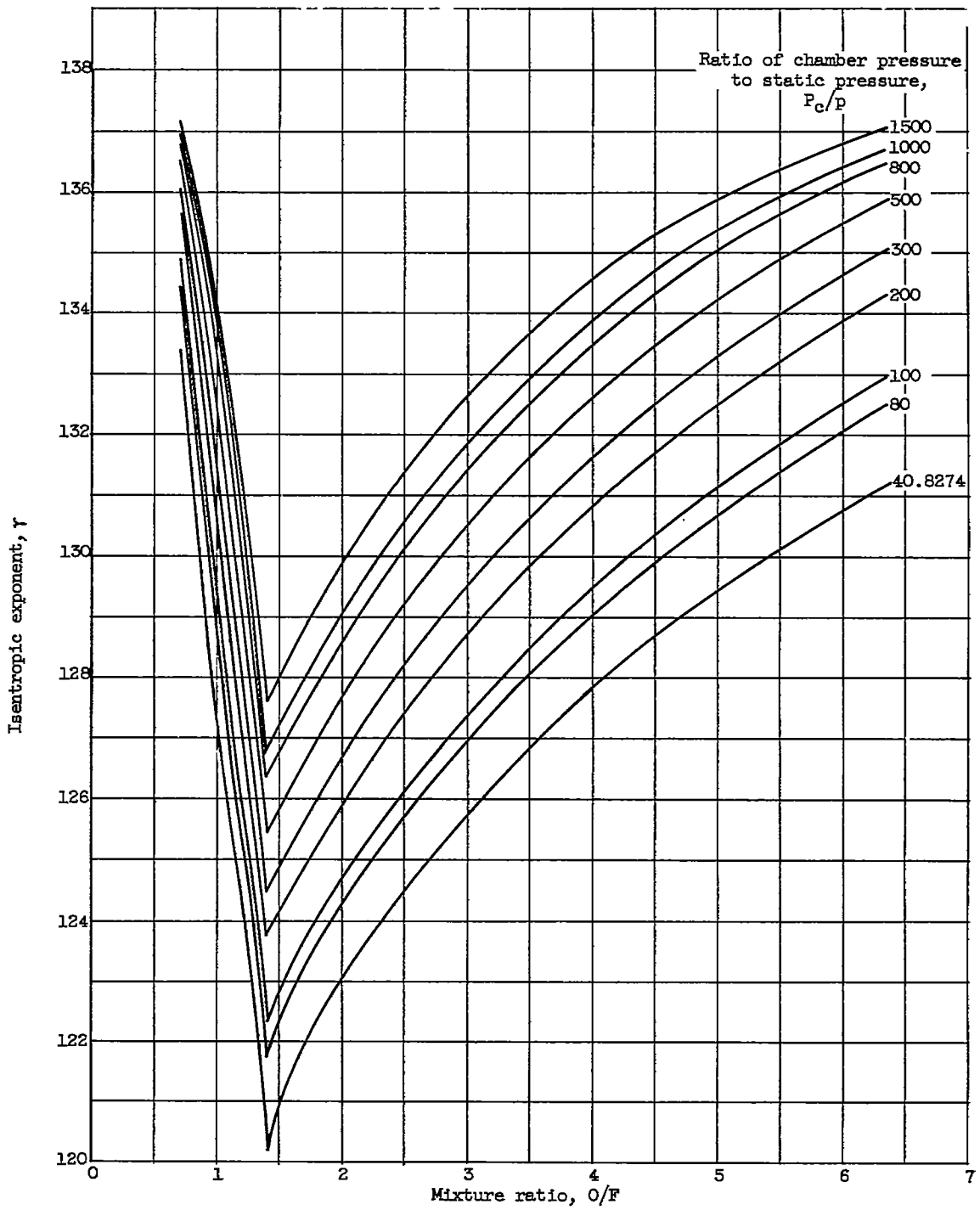

(b) Chemical equilibrium

Figure 23. - Concluded. Isentropic exponent as a function of mixture ratio for ammonia and oxygen.